THE EFFECT OF METAL ELECTRODES AND DEPOSITION ANGLE ON LINEARITY OF SCULPTURED TIO_2 HUMIDITY MICROSENSORS

by

Phenthai Phinmuang

A Dissertation Submitted in Partial Fulfillment of the Requirements for the Degree of Doctor of Philosophy in Microelectronics

Examination Committee:	Dr. Mongkol Ekpanyapong (Chairperson) Prof. Weerakorn Ongsakul Dr. Chaklam Silpasuwanchai
External Examiner:	Dr. Rawat Jaisutti Department of Physics, Faculty of Science and Technology, Thammasat University, Thailand
Nationality:	Thai
Previous Degree:	Master of Science in Physics Chulalongkorn University, Thailand
Scholarship Donor:	Thailand Graduate Institute of Science and Technology (TGIST) and AIT Fellowship

Asian Institute of Technology
School of Engineering and Technology
Thailand
May 2024

AUTHOR'S DECLARATION

I, Phenthai Phinmuang, declare that the research work carried out for this dissertation was in accordance with the regulations of the Asian Institute of Technology. The work presented in it are my own and has been generated by me as the result of my own original research, and if external sources were used, such sources have been cited. It is original and has not been submitted to any other institution to obtain another degree or qualification. This is a true copy of the dissertation, including final revisions.

Date: 29 April 2024

Name: Phenthai Phinmuange

Signature:

ACKNOWLEDGMENTS

First of all, I would like to gratefully acknowledge my advisor, Associate Professor Dr. Mongkol Ekpanyapong, for his valuable suggestions and kind support until this dissertation completed. Furthermore, I would like to thank all examination committees and the external committee for constructive comments to improve the quality of this research and dissertation report. Additionally, I would like to thank all officers at Asian Institute of Technology for providing information and convenience during the course of study.

In addition, I would like to sincerely express my gratitude Ms. Chalita Lertwinyu, Dr. Supanit Porntheerapat, Colonel Dr. Suwatwong Janchaysang, and Ms. Chowaret Sudsawaeng for their kind support and helps. There are many people from Asian Institute of Technology and Chulachomklao Royal Military Academy behind my achievement of the doctoral degree. I would like to thank all of those people that I cannot state here for their support. Importantly, I would like to thank my mother for her warm love which would push me forward along the journey of my life.

Furthermore, I would like to acknowledge Thailand Graduate Institute of Science and Technology (TGIST) for granting me a doctoral scholarship. I would like to thank Thai Microelectronics Center (TMEC) for providing instruments and laboratories. Lastly, I would like to thank Chulachomklao Royal Military Academy for giving me an opportunity to pursue my doctoral degree.

ABSTRACT

In this work, the linearity and sensitivity characteristics of capacitive-based titanium dioxide (TiO_2) humidity microsensors with various electrode materials have been studied. The TiO_2 thin films were produced using glancing angle deposition (GLAD) electron beam evaporator on either Ti or TiN microinterdigitated structure as contact electrodes. Using a field emission scanning electron microscope (FE-SEM), the produced thin films' crystallinity and surface morphology were evaluated. Additionally, the porous-like nanocrystalline TiO_2 films sculptured by GLAD and the anatase phase structure of TiO_2 thin films have also been investigated. By using the current-voltage and capacitance-voltage measurements, the sensitivity of TiO_2/Ti-electrode and TiO_2/TiN-electrode humidity sensors have been determined. As a result, the capacitive sensors using Ti electrodes exhibit superior linearity and sensitivity when compared to the sensors using TiN electrodes. For the sensors with Ti microinterdigitated electrodes and porous-like nanocrystalline TiO_2 films grown at 70° glancing angle, the sensitivity of 1.17×10^{-11} F/%RH and the linearity of 0.97 could be achieved.

CONTENTS

	Page
AUTHOR'S DECLARATION	**ii**
ACKNOWLEDGMENTS	**iii**
ABSTRACT	**iv**
LIST OF TABLES	**viii**
LIST OF FIGURES	**ix**
CHAPTER 1 INTRODUCTION	**1**
1.1 Background of the Study	1
1.2 Statement of the Problem	2
1.3 Research Questions	3
1.4 Objectives of the Study	3
1.5 Scope	3
1.6 Benefits	3
1.7 The Dissertation Overview	4
CHAPTER 2 LITERATURE REVIEWS	**5**
2.1 Nano-Particles of Titanium Dioxide	5
2.1.1 Nano-Particles	5
2.1.2 Nanometallic Particles	6
2.1.3 Properties of Nano Titanium Dioxide	6
2.2 Thin Film Preparation	12
2.2.1 Thin Film Deposition Process	17
2.2.2 Physical Vapor Deposition (PVD) Process	19
2.3 Growing Thin Film Nanostructures Using Glancing Angle Deposition (GLAD) Technique	25
2.3.1 Oblique Angle Deposition (OAD) Structure of Columnar Thin Films without Rotating Substrates	26
2.3.2 Film Growth Using the GLAD Technique	28
2.4 Principles of Film Property Analysis Tools	29
2.4.1 Study of Crystal Structure from X-Ray Diffraction (XRD)	29
2.4.2 Surface Analysis Using a Field Emission Scanning Electron Microscope (FE-SEM)	32

2.4.3 Studying Surface Topography with Atomic Force Microscope (AFM) 34
2.4.4 UV-VIS Spectroscopy for Studying Optical Properties 37
2.5 Principles of Moisture Sensor Measurement 40
2.5.1 Humidity 40
2.5.2 Humidity Sensor 42
2.6 Checking the Characteristics of a Moisture Sensor 43
2.6.1 Accuracy 43
2.6.2 Sensitivity 43
2.6.3 Linearity 43
2.6.4 Range 43
2.6.5 Resolution 44
2.6.6 Response 44
2.6.7 Frequency Response 44
2.6.8 Hysteresis 44
2.6.9 Repeatability 44
2.6.10 Stability 44
2.6.11 Reliability 45
2.6.12 Operating Life 45
2.6.13 Dual Sensitivity 45
CHAPTER 3 METHODOLOGY 46
3.1 Preparation of Thin Films Using Electron-Beam Evaporation in a Vacuum System 47
3.1.1 Components of the High Vacuum Electron-Beam Deposition System 48
3.2 Substrate Preparation 50
3.3 Titanium Dioxide Thin Film Growth 50
3.3.1 Steps and Conditions for Growing Thin TiO_2 Films 50
3.4 Preparation of Thin Film Tin-Dioxide Structure for Electrical Property Characterization 52
3.5 Characterization of Thin Film Tin-Dioxide Structure 53
3.5.1 X-Ray Diffraction Analysis for Structural Property Characterization 53

3.5.2 Discusses Examining Surface Characteristics Using a Field Emission Scanning Electron Microscope (FE-SEM) 53
3.5.3 Surface Analysis Using Atomic Force Microscope (AFM) 54
3.5.4 Checking Optical Properties with UV-VIS Spectroscopy 55
3.6 Testing of Electrical Properties 56
CHAPTER 4 EXPERIMENTAL RESULTS 58
4.1 Results of the Characterization of Nanostructured Thin Films of Titanium Dioxide 58
4.1.1 The Effect of the Angle between the Thin Film and the Substrate 58
4.1.2 The Effect of Room Temperature of Thin Films on Substrates 61
4.2 Examining the Specific Characteristics of the Humidity Sensor 62
4.2.1 Results of Optical Properties Examination 62
4.2.2 Results of Electrical Properties Examination 63
CHAPTER 5 CONCLUSIONS 67
REFERENCES 69
VITA 73

LIST OF TABLES

Tables		Page
Table 2.1	Important Physical Properties of Titanium Dioxide Nanoparticles	9
Table 2.2	Classification of Thin Film Growing Technologies	13
Table 2.3	Values of Wavelength, Energy, and Type of Excitation	40
Table 2.4	Comparison of Advantages and Disadvantages of Different Moisture Measurement Principles	42
Table 3.1	Conditions for Depositing Titanium Dioxide Films on Substrates a Different Angles	51
Table 3.2	Conditions for Baking Thin Films of Titanium Dioxide	51

LIST OF FIGURES

Figures		Page
Figure 2.1	Nanostructure of Titanium Dioxide (TiO_2)	6
Figure 2.2	The Generation of e- and h+ in TiO_2 When It Receives Light Energy	9
Figure 2.3	The Photocatalysis Process of the Titanium Dioxide Nanoparticles (TiO_2)	10
Figure 2.4	Energy Diagram of TiO_2 and the Redox Potential Corresponding to the Energy	11
Figure 2.5	Thin Film Preparation	12
Figure 2.6	The Process of Growing a Thin Film in a Vapor State	17
Figure 2.7	The Process of Small Atoms Clustering Together into Larger Clusters	18
Figure 2.8	The Film Formation Angle in Relation to Energy	19
Figure 2.9	Physical Vapor Deposition Process	20
Figure 2.10	Different Vapor Deposition Techniques	20
Figure 2.11	Types of Vapor Deposition System	21
Figure 2.12	The Types of Evaporation Sources	22
Figure 2.13	Electron Beam Control	24
Figure 2.14	The Design of a Substance Container	25
Figure 2.15	A Cross-Sectional View of the Origin of Electrons	25
Figure 2.16	The Arrangement of Equipment for the Oblique Angle Deposition (OAD) Technique	27
Figure 2.17	Shadowing Effect during Film Growth Using OAD Technique	27
Figure 2.18	The Arrangement of Equipment for Growing Films Using the GLAD Technique	28
Figure 2.19	X-Ray Diffraction from a Plane in a Crystal according to Bragg's Law	29
Figure 2.20	X-Ray Diffraction Pattern	31
Figure 2.21	Main Structure of Field Emission Scanning Electron Microscope	32
Figure 2.22	The Result of the Interaction between the Primary Electrons and Sample Atoms	33
Figure 2.23	The Cantilever Used for Measurements	34
Figure 2.24	Diagram of the Optical System Used to Measure the Bend of the Beam	34
Figure 2.25	The Atomic Force Microscope Measurement System	35
Figure 2.26	Force Distance Curve	36

Figure 2.27 The Nature of Light Transmission through a Medium 38
Figure 3.1 Diagram Showing the Research Process 46
Figure 3.2 System for Preparing Thin Films by Evaporation with Electron-Beam in Vacuum 47
Figure 3.3 Electron-Beam Vacuum Deposition System 47
Figure 3.4 The Inside of the Vacuum Container of the Film Preparation System 48
Figure 3.5 Control Panel of the Electron-Beam Evaporation System in the Atmosphere 49
Figure 3.6 Substrate Holder Used for Electron Beam Evaporation with Glancing Angle Deposition Technique 50
Figure 3.7 The Structure of the Thin Film Tin-Dioxide 52
Figure 3.8 Apparatus for Measuring Electrical Properties 52
Figure 3.9 An X-Ray Diffractometer (XRD) 53
Figure 3.10 A Field Emission Scanning Electron Microscope (FE-SEM) 54
Figure 3.11 Principles of Operation of an Atomic Force Microscope (AFM) 55
Figure 3.12 Atomic Force Microscope (AFM) 55
Figure 3.13 A UV-VIS Spectrophotometer 56
Figure 3.14 The Agilent E4980A Precision LCR Meter, 20 Hz to 2 MHz 57
Figure 4.1 X-Ray Diffraction Patterns of Thin Films of Nanocrystalline Titanium Dioxide at Different Angles 59
Figure 4.2 Photographs of the Surface and Cross-Section of Thin Films at Different Angles 60
Figure 4.3 The X-Ray Diffraction Patterns of the Nanocrystalline Titanium Dioxide Film at the Room Temperature of 70 Degrees 61
Figure 4.4 Photographs of the Surface of Thin Films the Room Temperature of 70 Degrees 62
Figure 4.5 The Light Absorbance of the Thin TiO_2 Films 63
Figure 4.6 The Examination of the Characteristics of Sensors with Different Relative Humidity and Temperatures during Baking on a Thin Film with 60 Degrees on a Supporting Base at the Room Temperature, with Varying Frequencies 64
Figure 4.7 The Examination of the Characteristics of Sensors with Different Relative Humidity and Temperatures during Baking on a Thin Film with 70 Degrees on a Supporting Base at the Room Temperature,

with Varying Frequencies 64
Figure 4.8 The Examination of the Characteristics of Sensors with Different Relative Humidity and Temperatures during Baking on a Thin Film with 80 Degrees on a Supporting Base at the Room Temperature, with Varying Frequencies 65

CHAPTER 1
INTRODUCTION

1.1 Background of the Study

In our daily lives, many people may overlook things that are close to us, such as temperature, weather conditions, or humidity. Many people can still live without needing to know the temperature or humidity levels at that time. However, for many other groups of people, communities, and organizations, this information is essential in their lives, especially in agriculture. Humidity is crucial for the environment and for growing various plants. We can use nanotechnology to produce small sensors made of titanium dioxide particles to measure humidity accurately in the air through the process of electron diffusion (Akbari-Saatlu et al., 2020; Aneesh & Khijwania, 2012). These sensors have special properties and high efficiency in measuring humidity in the air precisely, accurately, and quickly.

Excessive or insufficient humidity has a direct impact on the environment of our world and affects various aspects of the economy. Therefore, humidity is a major issue that researchers focus on solving and controlling according to the needs. This has led to the invention and development of various types of humidity sensors, each with unique characteristics and capabilities (Fang et al., 2004). This poses a challenge for new researchers who are trying to study and develop humidity sensors with special properties and high efficiency for use in addressing the problems that arise in traditional humidity sensors (Kuzubasoglu, 2022). This includes the use of new technologies and nanotechnology research in developing small-sized humidity sensors (Ku & Chung, 2023).

Small-scale moisture sensing education based on the structure of titanium dioxide metal oxide sheets through electron beam evaporation using nanotechnology is a research project that researchers are trying to study to develop efficient and high-performance moisture sensors (Aneesh & Khijwania, 2012). In addition, small-sized moisture sensors for portable use are also being developed.

The objective of this research project is to study small-scale moisture sensors to reduce limitations in traditional moisture sensing technology by using advanced technology to

study the best moisture sensors for measuring moisture in the air that is accurate, precise, and fast in processing. Currently, the use of nanotechnology in the production process of moisture sensors is closely related to this study of small-scale moisture sensing on the structure of titanium dioxide metal oxide sheets through electron beam evaporation, which is of great interest at present.

1.2 Statement of the Problem

There are many types of humidity sensors used in industry. When choosing to use a humidity sensor for different applications, there are some issues about humidity sensors that we should to consider, including

1. Accuracy
2. Repeatability
3. Stability
4. Condensation
5. Durability to chemicals
6. Size and package
7. Cost

A capacitive humidity sensor, a type of humidity sensor which can measure relative humidity and is widely used in industrial, commercial, research or physics experiments. This type of sensor has a structure consisting of a thin film base layer made of polymer. or metal oxide is placed between the two electrodes. The surface of the thin film is coated with a porous metal electrode to protect it from dust and sunlight (Das et al., 2003). Capacitive sensors can linearly measure the relative humidity in the environment, or there is a response in good proportion. For example, when the relative humidity value changes by 1%, the capacitance value is changed by 0.2 to 0.5 pF. Capacitive sensors are characterized by a low temperature coefficient that makes them work well. Even at temperatures as high as 200 °C, capacitive sensors can return to the original state from the condensation state and can be resistant to chemical vapors. Meanwhile, the sensor's response time is 30 to 60 seconds for humidity changes in the range of 63% (Liu et al., 2017).

Over the years, capacitive sensors have been developed with minimal drift and hysteresis, based on technology used to produce semiconductors. The new technology of conductors has been applied to produce thin film capacitive sensor. Some models of

capacitive sensors are also equipped with an input conversion circuit. This helps create a nearly linear electromotive force output that responds to changes in humidity values.

1.3 Research Questions

The research questions of this dissertation are discussed as follows:

1. can capacitive sensors with metal electrodes and TiO_2 thin films reduce limitations of traditional humidity sensors?
2. can capacitive sensors with metal electrodes and TiO_2 thin films measure humidity with better precision and accuracy?

1.4 Objectives of the Study

1. To study the properties of titanium dioxide nanoparticles
2. To study the system and methods for preparing thin films
3. To study the specific structural, surface properties, and light properties of the thin film of titanium dioxide nanoparticles for use as a moisture sensor

1.5 Scope

This research studies the properties of thin films of titanium dioxide nanoparticles and applies them to science and industrial work. The titanium dioxide nanoparticles are prepared through the electron beam evaporation process, where the thin film is deposited onto a silicon substrate under various conditions such as electric field strength to induce complete particle evaporation and varying distances to control the scattering of particles. The conditions for adjusting the distance during thin film preparation, the temperature of the substrate, and the time for thin film preparation are also investigated. The properties of the thin films are examined using the UV-VIS spectrophotometer method to analyze the structural characteristics based on light bending and create a moisture sensor. The important characteristics of the next sensor are then tested.

1.6 Benefits

1. Be able to understand the properties of titanium dioxide (TiO_2) nanoparticles.
2. Be able to understand the system and method for preparing thin films using electron beam evaporation.
3. Be able to understand the specific structural, surface, and optical properties of thin TiO_2 nanoparticle films. Can measure and analyze experimental results using X-ray diffraction (XRD), field emission scanning electron microscopy

(FE-SEM), atomic force microscopy (AFM), and UV-VIS is spectroscopy in sequence.

4. Be able to apply thin TiO_2 nanoparticle films as sensors for measuring humidity.

1.7 The Dissertation Overview

Chapter 1 will discuss the background and significance of the research, the research objectives, the scope of the research, and the benefits expected to be gained from the research.

Chapter 2 will discuss the basic theoretical foundations related to the research, which include the theory of titanium dioxide nanoparticles, the theory of thin film preparation through electron beam evaporation, and the theory of small-sized moisture sensor, which is the ultimate goal of this research.

Chapter 3 will discuss the various experimental methods of the research, starting from the process of preparing thin films of titanium dioxide nanoparticles through electron beam evaporation, including the checking of specific properties of the thin films using specific tools, and finally discussing the process of developing a small-sized moisture sensor.

Chapter 4 will discuss the results of the entire research process, from the preparation of thin films of titanium dioxide nanoparticles through electron beam evaporation, the results of checking specific properties of the thin films, and the results of checking specific characteristics of the small-sized moisture sensor.

Chapter 5 will summarize the results of the entire research process.

CHAPTER 2
LITERATURE REVIEWS

In this chapter, we will discuss the basic theory of nanomaterials and nanoparticles of titanium dioxide or devices at the nanometer scale that has new properties different from those of larger materials. We will cover the structural, surface, and optical properties of titanium dioxide nanoparticles.

In addition, this chapter also discusses the fundamental theory of thin film preparation technology, including the system for preparing thin films of titanium dioxide nanoparticles by evaporation of electrons using nanotechnology. This research has used this system to prepare thin films of titanium dioxide nanoparticles. We will then discuss the principles of small-sized film analysis tools, and finally, the theory of applying them as small-sized moisture measurement detectors, along with their important properties, in order.

2.1 Nano-Particles of Titanium Dioxide

2.1.1 Nano-Particles

Nano-particles are particles of a substance that have been designed to have a diameter smaller than 100 nanometers. This results in new properties or increased abilities compared to larger particles. For example, titanium dioxide (TiO_2) and zinc oxide (ZnO) can be transparent at the nano-scale, but still have the ability to absorb and reflect sunlight, so they are used in sunscreens and other chemicals (Aneesh & Khijwania, 2012). Nano-particles can also be used in paints, coatings for cars, clothing, blankets, and medical devices that can penetrate the skin to combat wrinkles. In addition to creating nano-particles from existing chemicals, nano-particles can also be combined with other materials (Barrettino et al., 2004). For example, creating nano-composite materials can accelerate reactions in industries. The development of nano-composite plastics that can selectively filter certain gases and steam to extend the freshness of fruits and vegetables, as well as increase their export value. Nanoparticles can also be used in medical equipment to kill bacteria, and viruses or make surfaces water-repellent (Niarchos et al., 2017).

2.1.2 Nanometallic Particles

Nanometallic particles such as gold, silver, and titanium nanoparticles possess unique properties, including surface plasmon resonance (SPR). Most nano metallic particles have SPR frequencies in the vicinity of the ultraviolet spectrum due to the excitation of free electrons on their surfaces, causing a plasmonic vibration.

2.1.3 Properties of Nano Titanium Dioxide

Nano titanium dioxide is a type of nanoparticle that belongs to the group of nano metallic particles. It has received significant research attention due to its numerous interesting properties that can be applied in various industries. It is non-toxic, has high stability, and is inexpensive, making it useful in many applications.

2.1.3.1 **Structural Properties of Titanium Dioxide Nanoparticles.** From various research studies on the nanoparticle structure of titanium dioxide, it can be found that there are three important crystalline structures, namely rutile, anatase, and brookite. Among these, the rutile structure of titanium metal has a tetragonal crystal structure and is the most commonly found in nature. It is durable and stable under high-temperature changes. Anatase has a tetragonal crystal structure and is a moderately found crystalline structure in nature. If heated above 915 degrees Celsius, the crystal structure changes to rutile. Brookite has an orthorhombic crystal structure and is the least commonly found crystalline structure in nature. It is stable under low-temperature changes. If heated above 750 degrees Celsius, the crystal structure changes to rutile (Shi et al., 2008).

Figure 2.1

Nanostructure of Titanium Dioxide (TiO_2)

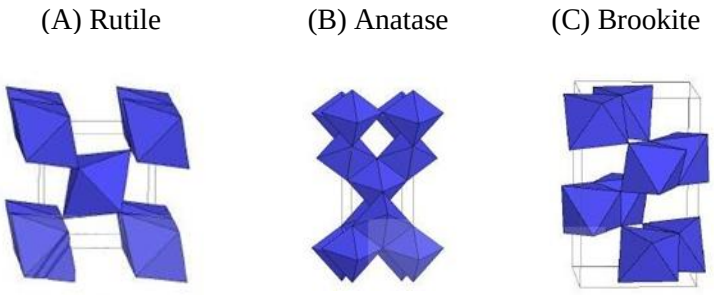

Source: (Boonnuk, 2011)

Currently, nanostructured titanium dioxide (TiO_2) particles are widely used for various purposes. They are often used in the form of rutile, a related mineral found in nature, in various industries. Meanwhile, the anatase type is often used in advanced light-related processes. The uses of TiO_2 nanoparticles in various fields are as follows:

Used as a Pigment:

The industry often uses TiO_2 nanoparticles as a component of house paint due to their white color properties, high light-scattering ability, and flexibility to cover cracks and wrinkles. They are also resistant to acid-base conditions, light, and heat. They are also used as a component of ink and art paint as they provide a bright white color.

Used as a Coating Agent:

TiO_2 nanoparticles are often used as coating agents in various industries such as plastic, glass, ceramics, metal, and paper. They reduce the penetration of light and are easy to adhere to the surface. They are also resistant to abrasion, which reduces the weight of the products.

Used as a Semiconductor in Electricity Production:

Solar cells commonly use titanium dioxide nanoparticles as a component, which is responsible for converting solar energy into electrical energy. It is used in the electronics industry, where it is often used as a capacitor due to its electrical properties, including a high electrical constant and high electrical resistance (Dai et al., 2005).

Used as a Component in Cosmetics:

It provides a fine white powder that has light-scattering and high-reflection properties, as well as good UV reflection without being harmful to the skin.

Used in Air and Water Pollution Control as an Adsorbent:

It acts as a substance that absorbs pollutants and accelerates the photochemical reaction. When exposed to light and heat, the titanium dioxide nanoparticles break down and produce substances and radiation that have many properties capable of eliminating waste or pollutants in water and air, as well as inhibiting and resisting bacteria, with the following mechanisms.

1. For the purpose of combating bacteria, when nanoparticles of titanium dioxide are exposed to light, they release hydroxyl radicals (OH+) and superoxide ions (O2-) into the air. These atoms then attract hydrogen and carbon atoms from the cell walls of the bacteria, as well as the organic compounds that cause odors and various toxic substances, causing them to break down.
2. To mitigate air pollution, such as nitrogen oxides (NOx), sulfur oxides (SO_2), and volatile organic compounds (VOCs), ultraviolet light in the range of 300-400 nanometers can be used to trigger a reaction between the aforementioned particles and pollutants. This reaction causes them to become nitric and sulfurous acids, while the volatile organic compounds undergo a structural change and become less hazardous.
3. To mitigate pollution in water, light can be applied to nanoparticles of titanium dioxide that are suspended in the water. When exposed to light, these nanoparticles release particles that react with the organic compounds in the water, causing them to turn into carbon dioxide gas, as shown in equation (2.1).

$$C_nO_mH + OH^+ + O^{2-} = nCO_2 + (n\text{-}m\text{-}1)\ H_2O \qquad (2.1)$$

2.1.3.2 Physical and Chemical Properties of Titanium Dioxide Nanoparticles.

The rutile, anatase, and brookite structures of titanium dioxide nanoparticles exhibit unique physical and chemical properties. These properties can be categorized as follows:

Physical Properties:

The rutile structure has the highest thermal stability, while the anatase and brookite structures are only stable at low temperatures. All three structures have important physical properties as shown in Table 2.1.

Table 2.1

Important Physical Properties of Titanium Dioxide Nanoparticles

Properties	Rutile	Anatase	Brookite
Crystal system	Tetragonal	Tetragonal	Orthorhombic
Density (g/cm^3)	4.24	3.83	4.17
Harness (Mohs scale)	5.50 – 6.00	5.50 – 6.00	7.00 – 7.50
Refractive index	2.71	2.52	-
Melting point (°C)	1,858	Changes to rutile at high temperature	-

Chemical Properties:

Both the anatase and rutile structures exhibit interesting chemical properties, specifically their ability to act as photocatalysts. When titanium dioxide nanoparticles are exposed to light in the ultraviolet region (with higher energy than the band gap energy), they absorb energy equal to the band gap energy, causing electrons in the valence band to be excited to the conduction band. This results in the presence of electrons in the conduction band (e-CB) and holes in the valence band (h+VB), as shown in Figure 2.2.

Figure 2.2

The Generation of e- and h+ in TiO_2 When It Receives Light Energy

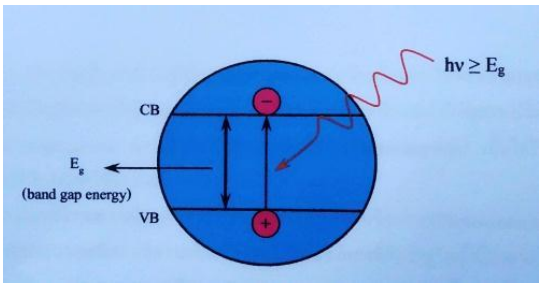

Source: (Boonnuk, 2011)

When the surface of a nanoscale titanium dioxide particle comes and touches with water (H_2O) and oxygen (O_2) present in the air, radicals with high reactivity are formed on the surface of the titanium dioxide nanoparticles. The molecules of water are oxidized and h+ is formed into hydroxyl radicals (Hydroxyl radical) as shown in equation (2.2).

$$h^+_{VB} + H_2O \rightarrow OH + H^+ \quad (2.2)$$

The hydroxyl radicals formed act as oxidizing agents with high energy that can decompose organic compounds absorbed on the surface of the titanium dioxide nanoparticles. Meanwhile, the molecules of oxygen are reduced by e- in the conduction band, becoming superoxide radical anions (Superoxide radical anion), as shown in equation (2.3).

$$e^-_{CB} + O_2 \rightarrow O_2^- \quad (2.3)$$

The superoxide radical anions formed act as reducing agents that can react with acceptor compounds absorbed on the surface of the titanium dioxide nanoparticles. This process is known as photocatalysis of the titanium dioxide nanoparticles, which is shown in Figure 2.3.

Figure 2.3

The Photocatalysis Process of the Titanium Dioxide Nanoparticles (TiO_2)

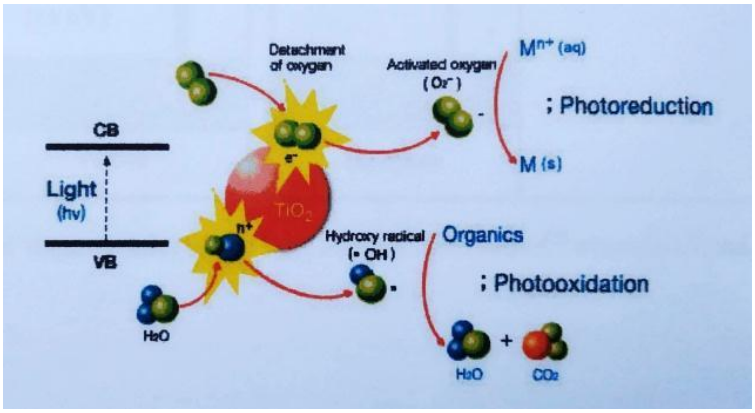

Source: (Boonnuk, 2011)

In addition to the photocatalytic property, titanium dioxide nanoparticles also exhibit a property called super-hydrophilicity, which causes a change in the surface from hydrophobic to hydrophilic when exposed to light energy from ultraviolet light.

From the experiment on photocatalysis, it was found that the anatase structure has better photocatalytic than rutile because the two structures have different band gap energy values. This energy value is the minimum light energy required to stimulate electrons to move. The band gap energy value of the anatase structure is 3.2 eV, corresponding to a wavelength of 388 nm, while the rutile has a band gap energy value of 3.0 eV, corresponding to a wavelength of 413 nm. Figure 2.4 shows that the anatase structure has a higher energy level of the conduction band than the rutile by 0.2 eV. The energy of the conduction band of the rutile structure is close to the threshold used to split water into hydrogen gas. However, the anatase structure has a higher energy level of the conduction band, making it better at splitting oxygen (O2) into superoxide radical anions (O2-) that can effectively decompose organic compounds, just like hydrogen peroxide.

Figure 2.4

Energy Diagram of TiO_2 and the Redox Potential Corresponding to the Energy

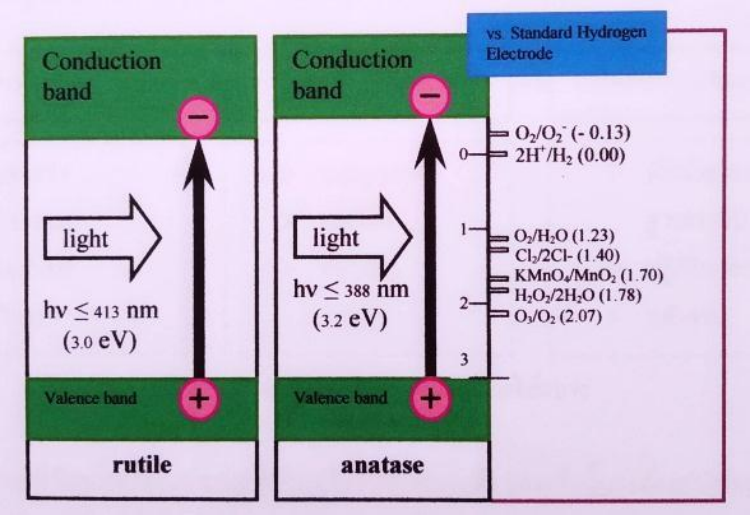

Source: (Boonnuk, 2011)

2.2 Thin Film Preparation

The process of producing thin films can be done in various ways and can be classified according to the state change of the material used to grow the film. Generally, the choice of material (source) for growing the film depends on its state, whether it is solid, liquid, gas, or vapor. The transport of the material to the substrate is also taken into consideration and can be done in a vacuum, fluid, or plasma state using various techniques. There are many methods for producing thin films, including physical vapor deposition and chemical vapor deposition, as shown in Figure 2.5.

Figure 2.5

Thin Film Preparation

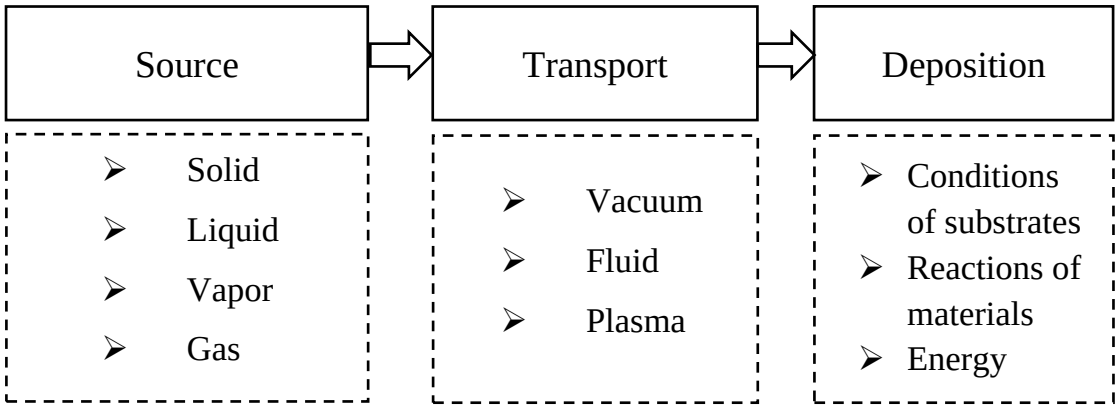

Preparation of thin solid films for use in modifying the surface properties of elements, scientific measurement tools, and electronic equipment (Miao et al., 2023). The process of electron beam evaporation is used to prepare films for use in nanotechnology and nanoelectronics. There are many methods for preparing films on a substrate, including:

1. Preparation of films on a substrate by preparing a solution and then evaporating the solvent.
2. Spray coating onto a substrate or applied to the preparation of metal layers.
3. Preparation of a film by compacting the vapor of a substance.
4. Preparation of a film by sputtering with radio frequency waves.
5. Using lasers to cut into layers.
6. Evaporation through chemical means.
7. Evaporation through physical means.

8. Using microwave plasma to coat layers.
9. Preparing a film by evaporating it into a frame-asis.
10. Preparing a film by using an electrochemical process to prepare metal films.
11. Preparation of films by spray coating with static electricity.

Table 2.2

Classification of Thin Film Growing Technologies

Thin film growing technology		
EVAPORATIVE METHODS	Vacuum Evaporation	Conventional Vacuum Evaporation Electron Beam Evaporation Molecular Beam Epitaxy (MBE) Reactive Evaporation
GLOW DISCHARGE PROCESSES	Sputtering	Diode Sputtering Reactive Sputtering Bias Sputtering (Ion Plating) Magnetron Sputtering Ion Beam Deposition Ion Beam Sputter Deposition Reactive Ion Plating Cluster Beam Deposition (CBD)
	Plasma Process	Plasma Enhanced CVD Plasma Oxidation Plasma Anodization Plasma Polymerization Plasma Nitridation Plasma Reduction

Thin film growing technology		
GLOW DISCHARGE PROCESSES	Plasma Process	Microwave ECR Plasma CVD Cathodic Arc Deposition
GAS PHASE CHEMICAL PROCESSES	Chemical Vapor Deposition (CVD)	CVD Epitaxy Atmospheric Pressure CVD (APCVD) Low Pressure CVD (LPCVD) Metalorgainc CVD (MOCVD) Photo Enhanced CVD (PHCVD) Laser Induced CVD (LICVD) Electron Enhanced CVD Ion Implantation
	Thermal Forming Process	Thermal Oxidation Thermal Nitridation Thermal Polymerization
LIQUID-PHASE CHEMICAL TECHNIQUES	Electro Process	Electroplating Electroless Plating Electrolytic Anodization Chemical Reduction Plating Chemical Displacement Plating Electrophoretic Deposition Liquid Phase Epitaxy
	Mechanical Techniques	Spray Pyrolysis Spray on Techniques Spin on Techniques

There are several ways to prevent the loss of a large amount of material due to adhesion to the vacuum chamber while spraying cadmium particles. Chemical vapor deposition and condensation of the vapor have been used. In cases where the material used to grow

the film is in a solid form, the solid must be converted into vapor before sending it to the substrate. Changing the state from solid to liquid, or from solid to vapor can be achieved by passing heat through electron beams, photons or ion beams. These methods are referred to as vapor-phase coating or physical vapor deposition (PVD), respectively. These methods are classified as vapor-phase coating or physical vapor deposition (PVD), respectively. For liquid or gas materials, there are chemical methods to convert them to vapor, which is called the gas-phase coating technique (Barrettino et al., 2004).

The transport of materials is an important factor in some thin film deposition processes, as there are significant differences between transport under a vacuum and transport in a high vacuum (Barrettino et al., 2004). In a high vacuum, molecules of the substance travel in a straight line from the source to the substrate, whereas in a flow system, molecule collisions occur during transport. Therefore, high vacuum deposition provides uniformity in the film growth. To achieve uniformity in the preparation of thin films, it is necessary to prepare thin films under high vacuum pressure. This allows gas molecules to be in a state of equilibrium, resulting in a uniform film.

$$P = \frac{1}{3}mn(v^2) \tag{2.4}$$

The equation above shows that the pressure of a gas is a function of the molecular mass (m), the number of molecules (n), and the square of the molecular velocity (v2), since mn represents the mass of the gas per unit volume, which is the density. Considering 1 mole of gas with a molecular mass of N0, volume V, and n = N0/V, we obtain:

$$P = \frac{1}{3}\frac{N_0}{V}m(v^2) \tag{2.5}$$

In the case of a 1 mol ideal gas which

$$PV = RT \tag{2.6}$$

so that

$$\frac{1}{2}mv^2 = \frac{3}{2}\frac{R}{N_0}T = \frac{3}{2}kT \quad (2.7)$$

The behavior of gas molecule movement while moving around will result in collisions with other molecules. The duration between one collision to the next is called the lifetime of the molecule, and the distance that the molecule travels during this time is called the mean free path. Since the time or distance between collisions can vary, finding the average values of these quantities is important. This is known as the mean lifetime and the mean free path, respectively. Therefore, the mean free path is the average distance between collisions.

$$l = \frac{\text{Number of times molecules traveled in time } dt}{\text{Number of times molecules collided in time } dt} \quad (2.8)$$

For gas atoms at room temperature, the collision-free mean l is equal to

$$\lambda = \frac{k_B T}{\sqrt{2}\sigma P} \quad (2.9)$$

Where l is the cross-section in the collision of gas atoms which has a range of 10^{-16} cm^2 and P is the pressure in the case where T = 300 K and σ = 4 x 10^{-15} cm^2 Mean free path is equal to

$$\lambda = 0.7cmP^{-1} \quad (2.10)$$

where P is the pressure in atmospheric pressure (atm).

In other words, the collision-free mean means the atomic flux acting on the surface. In the case of an ideal gas, flux and pressure can be expressed by

$$F = \frac{P}{\sqrt{2\pi m k_B T}} \quad (2.11)$$

where m is the mass of gas particles, or

$$F = 2.63 \times 10^{17} \frac{P}{\sqrt{mT}} cm^{-2}s^{-1} \quad (2.12)$$

The mean free path is important in preparing thin films because in the case of vapor deposition if the substance is evaporated under very low pressure, it may result in a thin film of high quality, which means that gas molecules have fewer collisions. Therefore, the movement towards the substrate is orderly. Comparing vapor deposition under different pressures can determine that a thin film prepared under higher pressure may not give good results, such as unclear edges of the thin film during the deposition process. The movement of these substances during the formation of a thin film is an important variable that determines the structure of the thin film in the final step. If the substance can move or spread well, it increases the chance of atoms arranging themselves in an orderly manner on the substrate.

2.2.1 Thin Film Deposition Process

The thin film deposition process involves several important steps, including:

2.2.1.1 **Adsorption Process.** The first process in the formation of a thin film on the surface of the substrate is the adsorption process. When molecules move into the surface of the substrate, in the initial stage, physisorption occurs due to the occurrence of van der Waals forces. Therefore, when the molecules are absorbed and spread onto the surface, in the next step, chemisorption occurs.

Figure 2.6

The Process of Growing a Thin Film in a Vapor State

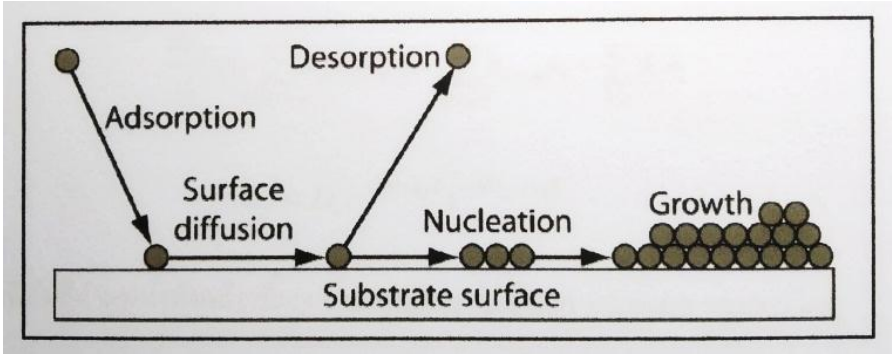

Source: (Boonnuk, 2011)

2.2.1.2 **Desorption Process.** The process of desorption refers to the release of molecules from the surface of the substrate upon impact or for other reasons. For example, when the growth time of a film is increased and the atoms are densely packed, some atoms will be released from the densely packed region.

2.2.1.3 **Nucleation Process.** The nucleation process begins with a gas molecule colliding with the surface of the substrate. At the same time, another gas molecule enters the surface of the substrate. When the two molecules combine, they form a diatomic molecule, and they begin to group together as the distance between the substrate surfaces decreases, forming larger clusters. The key factor in the nucleation process is surface diffusion.

Figure 2.7

The Process of Small Atoms Clustering Together into Larger Clusters

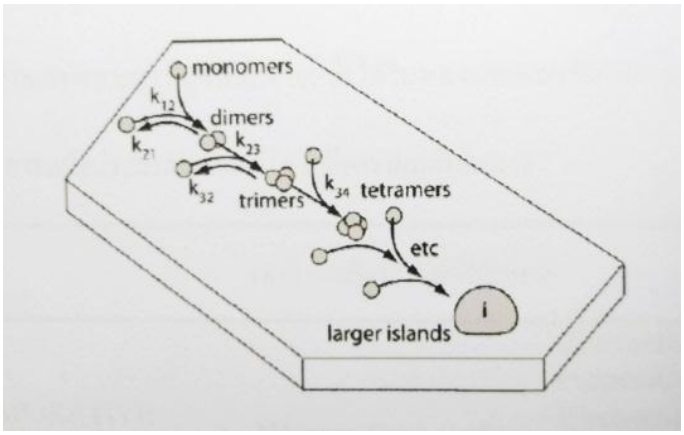

Source: (Boonnuk, 2011)

2.2.1.4 **Film Growth Process.** This process begins with the clustering of atoms and their dense packing. The rate of film growth per unit of time is determined by the equation. (the remainder of the text is not provided).

$$\frac{dn_i}{dt} = \sum_{0<j<i-j} k_{j,i} n_j n_{i-j} - \sum_{0<m<i} k_{i,i-m} n_i - \sum_{l>i} k_l n_l \quad (2.13)$$

$$k_j = D_0 e^{-ED/k_B T} e^{-\Delta G_{j,i}/k_B T} \quad (2.14)$$

In the film formation at this location Can study the mismatch of substances by

Figure 2.8

The Film Formation Angle in Relation to Energy

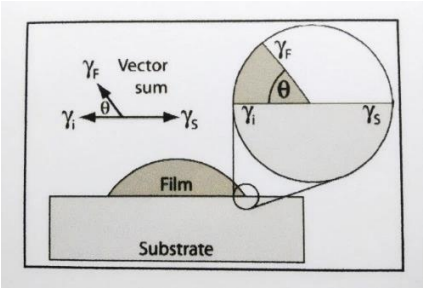

Source: (Boonnuk, 2011)

2.2.2 Physical Vapor Deposition (PVD) Process

Physical Vapor Deposition (PVD) refers to the process of evaporating material and allowing it to condense on a substrate to form a thin film. This technique involves the physical evaporation of a solid material and its subsequent deposition on a substrate under vacuum conditions. Physical evaporation can be achieved by a variety of methods, such as sputtering or evaporation using thermal energy.

Sputtering is a physical process that involves bombarding a target material with high-energy ions to release atoms from its surface, which then deposit on the substrate. Laser ablation is another physical process that is similar to evaporation, except that the energy source used to evaporate the material is a laser beam. Cathodic arc deposition is another physical process that is similar to sputtering, but instead of ions, a cathodic arc is used to evaporate the material.

Compared to chemical vapor deposition (CVD), PVD processes operate at lower temperatures and can produce highly uniform and dense films. PVD techniques are widely used in the microelectronics and semiconductor industries, as well as in the production of coatings for cutting tools, automotive parts, and decorative finishes (Dai & Yu, 2006). The PVD process for growing thin films is shown in Figure 2.9.

Figure 2.9

Physical Vapor Deposition Process

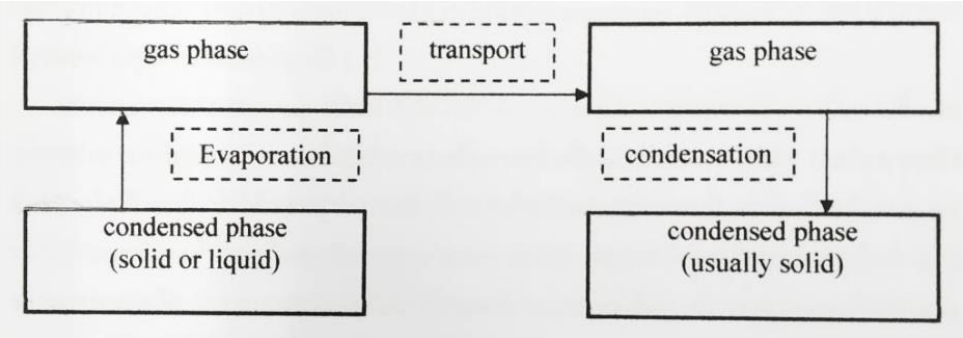

There are various methods to prepare thin films using physical vapor deposition techniques, such as co-evaporation, sequential deposition, sputtering, and pulsed laser deposition. The different PVD systems have different mechanisms for vaporizing and depositing materials, as shown in Figure 2.10.

Figure 2.10

Different Vapor Deposition Techniques

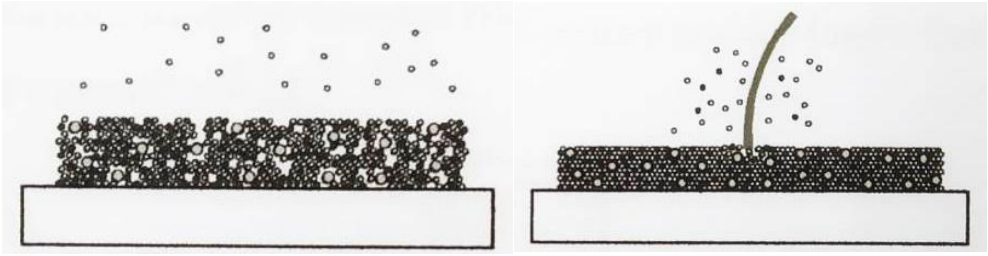

(a) Thermal Evaporation (b) Electron Beam

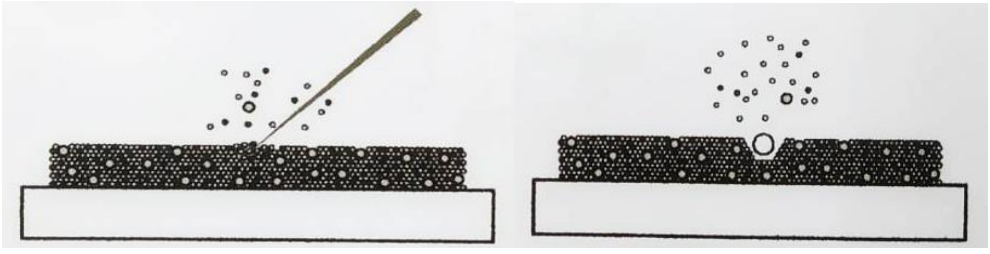

(c) Pulsed Laser (d) Sputtering

Source: (Boonnuk, 2011)

2.2.2.1 **Vapor Deposition Technique.** There are several types of vapor deposition systems, ranging from simple systems that use an electric current to heat a wire and create a vapor in a vacuum chamber to more complex systems, such as molecular beam epitaxy (MBE), that can precisely control the deposition process at the molecular level. MBE is a high-precision system that can control the molecular beam in ultra-high vacuum conditions of less than 10^{-9} Pa or 10^{-14} atm. Although MBE has many advantages, it is also expensive compared to other vapor deposition systems. All vapor deposition systems include a vacuum chamber, a pump to evacuate the chamber, a source for vaporizing the material, and various electronic control and monitoring systems to regulate the deposition process, such as measuring the flux of atoms (Miao et al., 2021), as shown in Figure 2.11.

Figure 2.11

Types of Vapor Deposition System

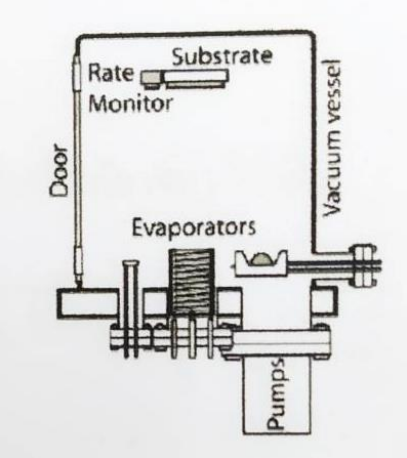

Source: (Boonnuk, 2011)

"Source" is the entity that provides heat to the substance undergoing evaporation. The method of selecting a source depends on the phase of the substance being evaporated, which includes wire sources that are electrical resistors. There are many types of electrical resistors, such as those that are in the form of a sheet and can be made from various materials such as tungsten and molybdenum. Other sources of evaporation, such as those used for electron beam evaporation, have a crucible-like shape. In the case of organic substances, there is a cooling surround around the crucible. This shape is

suitable for substances with low melting points, such as organic materials, which are a type of substance that can be evaporated.

Figure 2.12

The Types of Evaporation Sources

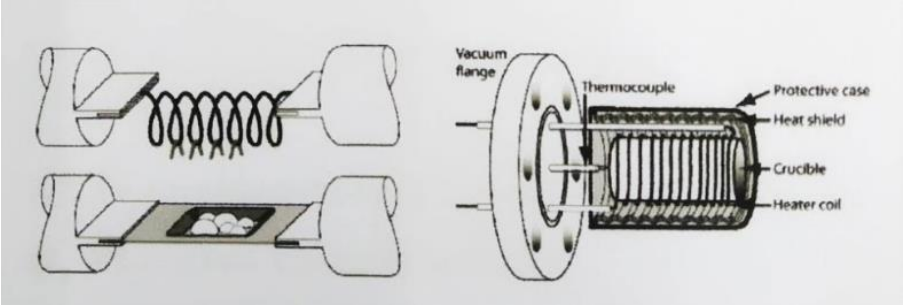

Source: (Boonnuk, 2011)

In the evaporation system, a deposition monitor must be used to measure the thickness of the film. There are generally three methods of measuring thickness, which are:

1. Mass deposition, which causes a change in the frequency of the substance being used as a probe to measure moisture.
2. Change in light reflection while the thickness of the film is increasing.
3. Using the principle of Reflection High-Energy Electron Diffraction (RHEED), which is a method used in the process of growing an atomically arranged film.

The method commonly used in the evaporation system is the mass deposition method, which uses a crystal sheet that vibrates at a certain frequency. Then, when the aforementioned thin film is deposited, the substance undergoing evaporation will adhere to the crystal sheet, causing the frequency of the crystal sheet to change. This change in frequency is used to calculate the thickness of the thin film.

$$f_r = \frac{1}{T_v} = \frac{1}{2\pi}\sqrt{\frac{k}{m}} \qquad (2.17)$$

where f_r is the resonant frequency (Hz).

T_v is the vibration period (s)

k is the spring constant (N/m).

m is mass (kg)

When a substance is coated on a crystal plate The equation can be written as follows:

$$T_v = T_{vo} + \Delta T_v \ \alpha \ \sqrt{m_q + m_f} = \sqrt{m_q\left(1+\frac{m_f}{m_q}\right)} = \sqrt{m_q}\left(1+\frac{1}{2}\frac{m_f}{m_q}\right) \tag{2.18}$$

So that

$$T_v \ a \ m_f \ a \ r_f h_f \tag{2.19}$$

where $\triangle T_v$ refers to the changes in the deposition rate and loading weight

m_q refers to the weight without coating (kg)

m_f refers to the weight after coating (kg)

ρ_f refers to the density of the coating material (kg/m^3)

h_f refers to the thickness of the coating or evaporation (m)

Important parameters for the evaporation of the substance include:

1. Mass deposition rate
2. Uniform coating.

2.2.2.2 **Electron Beam Evaporation System in Vacuum.** The principle of the electron beam evaporation system in a vacuum is to control electrons with a magnetic or electric field so that they fall onto the substance to be evaporated in a crucible linear. Electrons are generated by feeding an electrical current to a tungsten filament until the thermionic emission effect occurs. Electrons are released and forced to collide with the surface of the substance, resulting in the transfer of energy. This energy is converted from electrical energy to thermal energy, causing the substance to change state from solid to gas. The evaporated substance is deposited onto a substrate and the crystal structure is formed by changes in the frequency of vibration of the deposited substance. The electron beam is generated by the flow of electrical current through a filament, which then releases electrons. The direction of the electron beam is controlled by a

magnetic field, directing the electrons onto the crucible of the substance to be evaporated.

Figure 2.13

Electron Beam Control

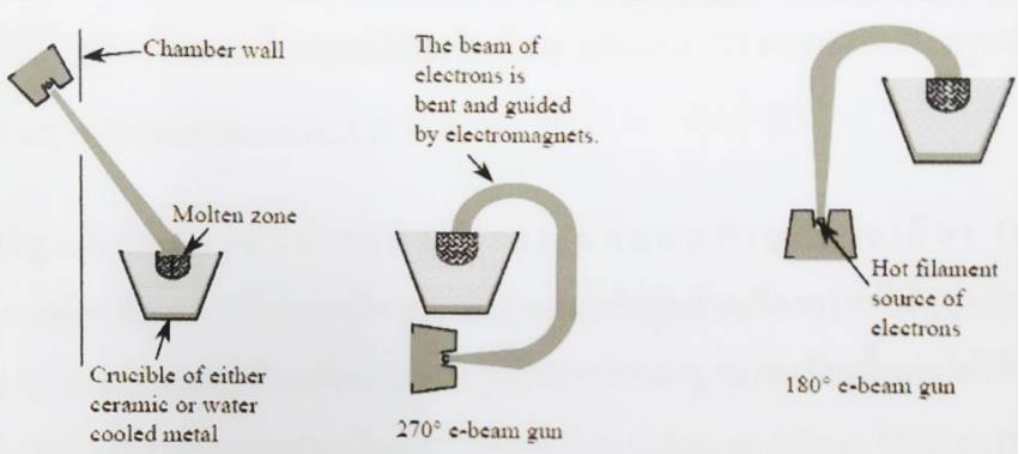

Source: (Boonnuk, 2011)

There are various types of electron beam technology designed for use in industry or research. In some cases, electron beams are used to melt materials. Examples of this are shown in images 2.14 and 2.15. When using the same type of film, a single crucible should be selected for continuous use. In research, multiple crucibles may be used when growing thin films, depending on the specific requirements. After the first layer of material is completed, the crucible containing the material is rotated to the next layer, making this method convenient for growing multi-layered films. An example of growing thin films is the process of growing chromium (Cr) layers for adhesion between gold (Au) and the surface of a material in electronic devices.

Figure 2.14

The Design of a Substance Container

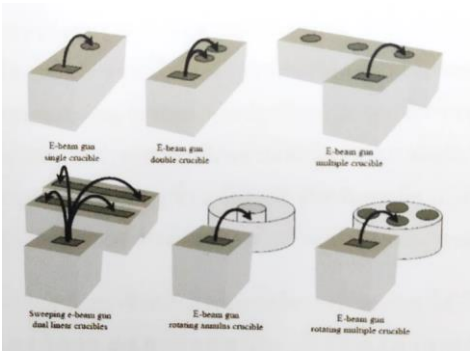

Source: (Boonnuk, 2011)

Figure 2.15

A Cross-Sectional View of the Origin of Electrons

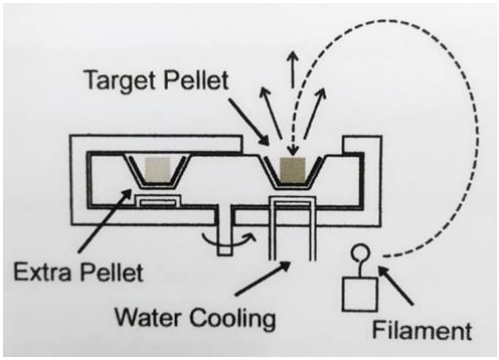

Source: (Boonnuk, 2011)

2.3 Growing Thin Film Nanostructures Using Glancing Angle Deposition (GLAD) Technique

Growing thin films using the Glancing Angle Deposition (GLAD) technique is a method that combines the growth of thin films with the glancing angle deposition technique without rotating the substrate together with controlling the position of the substrate (Vrakatseli et al., 2018). This creates films with various nanostructure shapes that can be controlled in terms of pore size and shape. GLAD is a physical vapor deposition process, in which the vapor can collide with the substrate at a large angle, depending on the surface and rotation of the substrate. The GLAD technique creates a

columnar structure due to the shadowing effect during film growth and the control of the shape of the column during the GLAD process by rotating the substrate. The side growth rate causes the shadowing effect, which is the main advantage of GLAD technique: the self-alignment effect and the lateral sculpturing effect. There are three main factors that can determine the structure of the column: the angle of incidence of the vapor, the deposition rate, and the speed of the substrate rotation. Changing the angle can create C-shape, S-shape, and zigzag-shaped columns. Changing the deposition rate and rotation speed can create rectangular columns, twisted columns, and straight columns (Kraus et al., 2003). The advantages of the GLAD technique are:

1. It can create nano-sized columns with controlled pore size and shape.
2. It can produce 3D structures on a large scale.
3. It can be applied to various materials, including metals, semiconductors, and polymers.

2.3.1 Oblique Angle Deposition (OAD) Structure of Columnar Thin Films without Rotating Substrates

The arrangement of equipment for the OAD technique is shown in Figure 2.16, with the direction of deposition arranged at a wide angle to the normal surface of the substrate. Therefore, it is necessary to control both the deposition of the impacting vapor and the deposition of the vapor that is parallel to the substrate surface. These two types of vapor deposition can be divided into two parts: the vapor deposition that is perpendicular to the substrate surface (F_{pe}) and the vapor deposition that is parallel to the substrate surface (F_{pa}). The vapor deposition has two components: the vertical component $F_{pe} = F \cos \theta$ and the lateral component $F_{pa} = F \sin \theta$. The substrate can receive vapor deposition from both directions, i.e. vertically and laterally.

Figure 2.16

The Arrangement of Equipment for the Oblique Angle Deposition (OAD) Technique

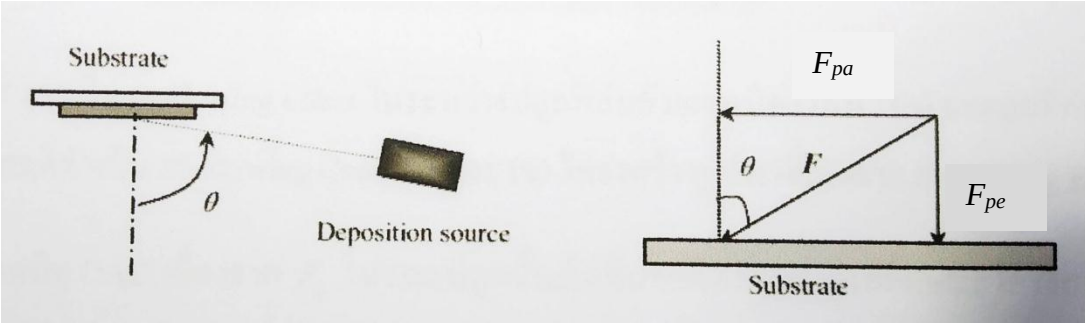

Source: (Boonnuk, 2011)

During the film deposition on a flat substrate, atoms initially impinge freely onto the substrate surface, as shown in Figure 2.17. The formed cluster of material known as "islands" behave as shadowing centers. The highest islands receive more impinging atoms than lower ones, resulting in a shadowing effect. Eventually, only the highest islands become nanoscale columns that form thin films with a columnar nanostructure. The sidewalls of the columns are the source of the shadowing effect (Xiaowei et al., 2011).

Figure 2.17

Shadowing Effect during Film Growth Using OAD Technique

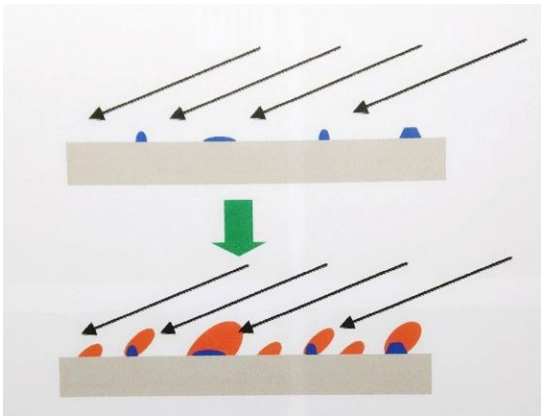

Source: (Boonnuk, 2011)

For the OAD technique, since F_{pa} during the film growth, as there are random occurrences. Some thin films exhibit a structural feature of inclined columns β. The structure of these columns in thin films β is generally inclined at a smaller angle than the angle of incidence of the vapor flux and follows the law of Tangent, as shown in equation (2.20),

$$\tan\beta = \frac{1}{2}\tan\theta \tag{2.20}$$

or the law of Cosine, as shown in equation (2.21)

$$\beta = \theta - \arcsin\left(\frac{1-\cos\theta}{2}\right) \tag{2.21}$$

Thin films grown using the OAD technique have properties such as porous structures and nano-sized columnar structures (Furjes et al., 2003). These columnar structures are inclined from the normal surface direction according to the angle of incidence of the vapor flux, size, and density of the nano-sized columns, which change with the angle of incidence.

2.3.2 Film Growth Using the GLAD Technique

Although some thin films have columnar structures created by the OAD technique, which are considered to be a nanostructure, the structure that is created is not easy to control during the growth process (Xiaowei et al., 2011). Typically, inclined columns are developed from the OAD technique, as shown in Figure 2.18.

Figure 2.18

The Arrangement of Equipment for Growing Films Using the GLAD Technique

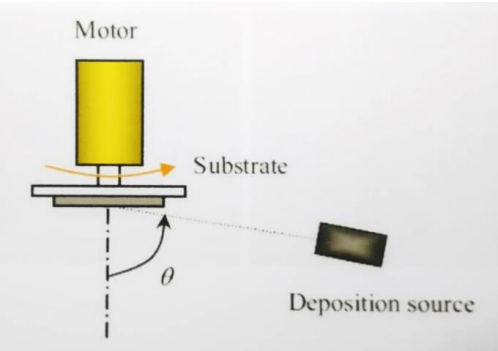

Source: (Boonnuk, 2011)

The basic setup for growing films is similar to the OAD technique, but the support base has two stepper motors. One motor controls the angle of impact and the other controls the circular rotation in the horizontal plane of the support base. During the growth process, the support base can rotate in a circular motion in the horizontal plane, with the angle of impact set at one angle or changing as the base rotates. The movement of the two motors is controlled by a computer, which changes the speed and phase of the rotation in the horizontal plane and the back-and-forth motion. The combination of the two rotations and the growth rate allows for the creation of nanometer-scale shapes such as C-Shape, S-Shape, and Zigzag Shape.

2.4 Principles of Film Property Analysis Tools

2.4.1 Study of Crystal Structure from X-Ray Diffraction (XRD)

X-ray diffraction is a method used to study the crystal structure of films, which tells us the lattice constant of the film and the planes present in the X-ray diffraction pattern. X-rays are electromagnetic waves with high energy and wavelengths between 0.5 and 2.5 angstroms, generated by accelerating electrons in an electric field and colliding them with a heavy metal such as gold. X-rays produce two types of radiation: continuous X-rays and characteristic X-rays. X-rays exhibit wave properties, namely diffraction when passing through gaps between atoms in a crystal structure, and after the waves pass through the crystal structure, both constructive and destructive interference occurs. If only the area where the X-ray beam hits the atom is considered, X-rays exhibit particle-like properties, namely scattering in all directions when the X-ray beam interacts with the atoms arranged on the plane of this crystal structure, which acts as if the X-ray beam that strikes it is being reflected.

Figure 2.19

X-Ray Diffraction from a Plane in a Crystal according to Bragg's Law

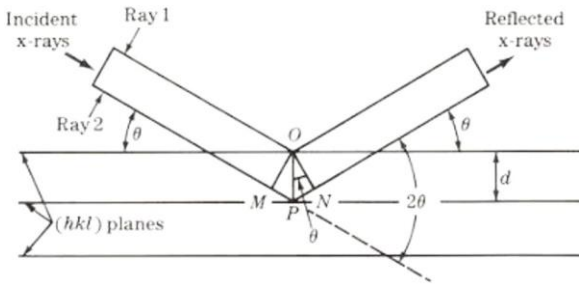

When the X-rays strike the plane of the crystal where the distance between the planes is d. X-rays incident at points O and P make an angle with the plane and are reflected from the plane at an angle θ. The path difference of the two X-rays is MP + PN, which is $2d \sin \theta$. By interfering Complementary radiation can occur when the path difference must be equal to $n\lambda$, where n is an integer and λ is the wavelength of the X-rays. It can be expressed as equation (2.22).

$$2d_{hkl} \sin \theta = n\lambda \tag{2.22}$$

where = diffraction order is from 1, 2, 3, …

Equation (2.22) is called Bragg's law in crystallography, which describes a crystal lattice as composed of different atomic planes. The planes are specified using symbols (hkl), which hkl are called Miller indices and are integers starting from 0, 1, 2, ... The distance between the planes in the same set depends on the Miller indices (hkl) and the constant values of the crystal lattice (a, b, c, α, β, γ). The relationship between the distance between the planes and the constant values of the crystal lattice varies according to different crystal systems.

In the simple case of a crystal structure with a Cubic lattice, where the lattice constants are a = b = c, $\alpha = \beta = \gamma = 90°$ the relationship is as follows:

$$d_{hkl} = \frac{a}{\sqrt{h^2+k^2+l^2}} \tag{2.23}$$

where a is the lattice constant.

λ is the wavelength of X-rays.

θ is the angle of diffraction.

In crystallography, various planes in a crystal lattice do not cause continuous X-ray diffraction. The plane that causes diffraction according to Bragg's law is called a Bragg plane. The angle between the incident X-ray and the Bragg plane is called the diffraction angle, which is twice the angle of reflection. By measuring the intensity of

the X-ray diffraction and the diffraction angle using an X-ray diffractometer, the intensity and diffraction angle can be analyzed to obtain a diffraction pattern. The diffraction pattern is a unique characteristic of a particular element or compound. Once the diffraction pattern is obtained, it is possible to calculate the lattice constant of the crystal structure of the material.

Figure 2.20

X-Ray Diffraction Pattern

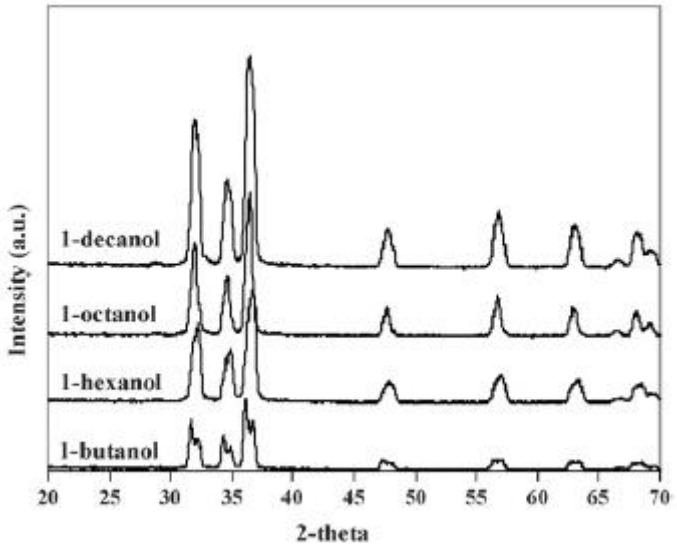

From the Sherrer's equation, the grain size can be obtained as follows:

$$D = \frac{K\lambda_X}{\beta_{2\theta}\cos\theta} \tag{2.24}$$

where D is the grain size.

K is a constant that depends on the size and shape of the crystal ($0.89 \leq K \leq 0.94$)

θ is the angle of diffraction.

$\beta_{2\theta}$ is half the maximum width of the diffraction peak.

λ_X is the wavelength of X-rays.

2.4.2 Surface Analysis Using a Field Emission Scanning Electron Microscope (FE-SEM)

The working principle of a Field Emission Scanning Electron Microscope (FE-SEM) can be seen from Figure 2.21, which can explain the operation of the FE-SEM as follows. The electron gun, which has three types of cathodes: tungsten, Lanthanum hexaboride (LaB6), and field emission, produces electrons from the filament and accelerates them with an electric field in the range of 1-40 kV. The resulting electron beam is focused by the condenser lens and adjusted for focus by the objective lens. If it is desired to scan the electron beam across the surface of the sample, scanning coils can be used to scan the beam in the x-y plane, creating a signal that is then detected by the detector. The detector measures the signal and converts it into the desired data using an electronic system. When the electron beam from the electron source is focused onto the surface of the sample, an interaction occurs between the electrons that are shot down and the atoms of the sample. This interaction can be divided into two types: elastic and inelastic. Both types of interactions provide different signals for use.

Figure 2.21

Main Structure of Field Emission Scanning Electron Microscope

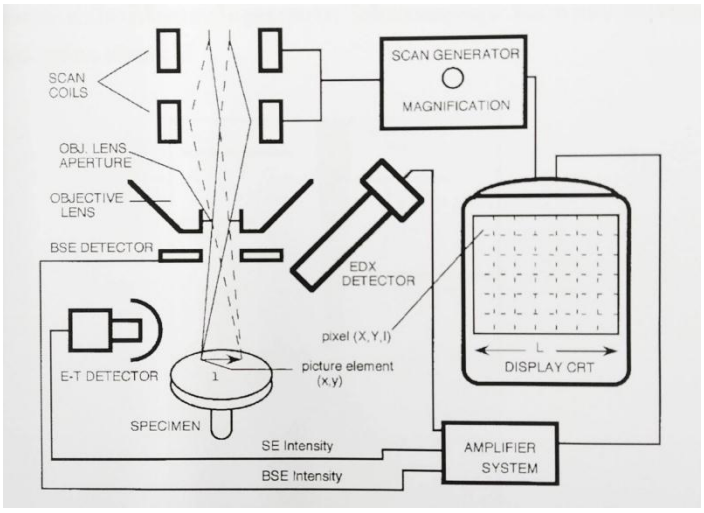

Source: (Boonnuk, 2011)

2.4.2.1 **Elastic Scattering.** When the electrons group from the electron source, the primary electron falls on the sample, causing the electrons to come out. Some energy loss, which is very small to the atoms of the sample The electrons are scattered. We call it Backscatter Electron, which can be used as a video signal on CRT.

2.4.2.2 **Inelastic Scattering.** The group of primary electrons, when collided with the atoms of the sample. The kinetic energy will occur and the interaction with the sample atoms, causing signs that Detector can measure, including Secondary Electron, Auger Electron, Characteristics X-ray, Continuous X-ray and Fluorescence X-ray, etc. Following to Figure 2.22 Secondary Electron is caused by primary electrons, shooting energy for different electron electrons (Shell) of the sample atoms. If the energy provides more than the energy of the electrons in the orbits and the nucleus of the sample atom will cause the electrons in the orbit to come out. We call the electrons that come out Secondary electrons, which can be used to study the face of the sample.

Figure 2.22

The Result of the Interaction between the Primary Electrons and Sample Atoms

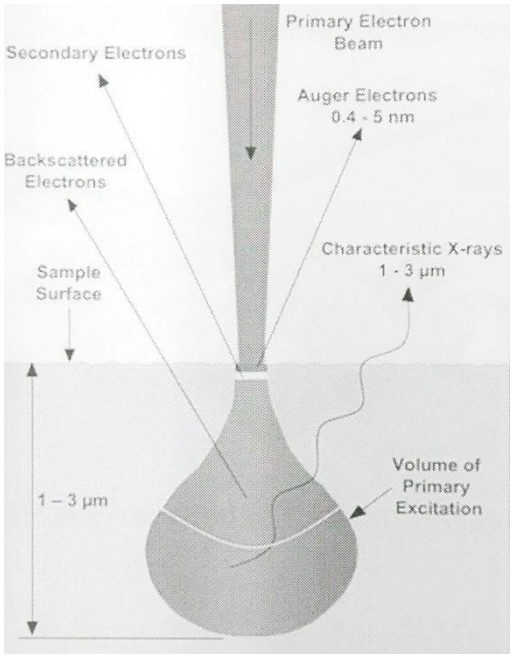

Source: (Boonnuk, 2011)

2.4.3 Studying Surface Topography with Atomic Force Microscope (AFM)

The Atomic Force Microscope (AFM) was invented in 1986 by Binnig, Quate, and Gerber. It uses a sharp probe to scan across the surface of a sample. The probe, also known as a cantilever, has a small pointed tip at its end. The cantilever is able to bend and move in response to the forces between the tip and the sample surface.

Figure 2.23

The Cantilever Used for Measurements

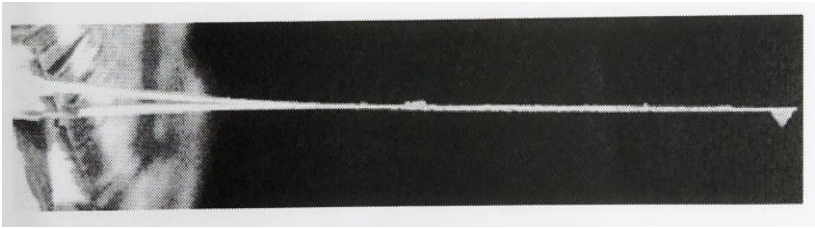

Source: (Boonnuk, 2011)

Initially, the AFM used electron tunneling through the cantilever's deflection to measure the sample's topography. However, modern AFM uses light-based techniques to detect the cantilever deflection, as shown in Figure 2.24. Laser light is reflected off the cantilever onto two photodetectors, which measure the difference in signal to determine the cantilever's deflection. This method allows for precise measurement of the sample's topography, even at the atomic scale.

Figure 2.24

Diagram of the Optical System Used to Measure the Bend of the Beam

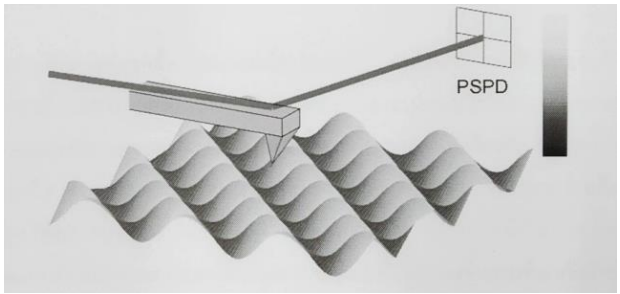

Source: (Boonnuk, 2011)

The movement of a high-precision needle or workpiece is achieved using equipment made from ceramic piezoelectric materials. Changes occur due to the electrical energy that stimulates them, which is mostly in the form of a cylindrical shape. The motion controller can control the movement with high precision in the x, y, and z-axes, where the z-axis is perpendicular to the workpiece (Yadav et al., 2011).

Figure 2.25

The Atomic Force Microscope Measurement System

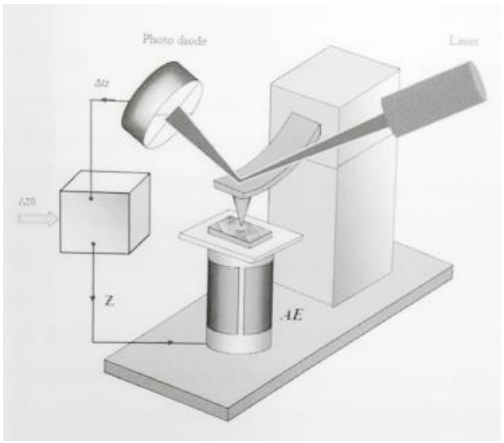

Source: (Boonnuk, 2011)

It can operate in two main modes: feedback-controlled mode and non-feedback-controlled mode. In the feedback-controlled mode, the piezo is used to control the movement of the workpiece or needle, enabling it to move up and down while maintaining a constant distance between the needle and the workpiece. This mode is called the constant force mode, which allows for reliable imaging of the surface characteristics of the workpiece.

Figure 2.26

Force Distance Curve

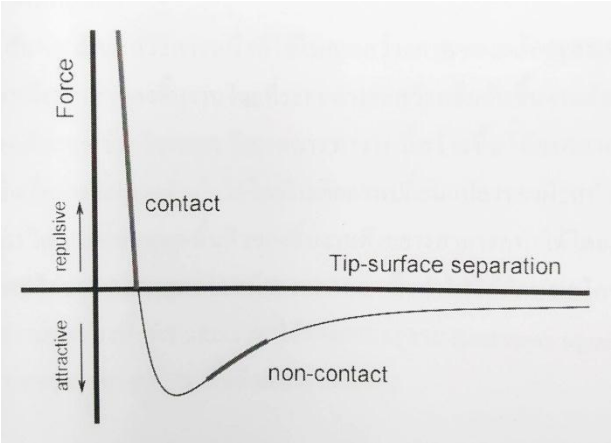

Source: (Boonnuk, 2011)

The second operating mode does not have feedback control and is a mode that controls movement in a fixed position along the z-axis and measures the bending of the cantilever. This mode is useful for samples that have a very smooth surface and require high resolution.

There are several ways to obtain an atomic force microscopy image using the different interactions that occur between the tip and the sample. The three main modes used to measure atomic forces are constant force mode, tapping mode, and non-contact mode.

Constant force mode is a commonly used basic method of atomic force microscopy, where the tip and sample are brought very close to each other while the tip is scanned over the sample. The interaction between the tip and sample occurs when they are very close, and this area corresponds to the area above the x-axis on the graph. The main problem with constant force mode is that there is a large force acting on the surface of the sample when the tip is scanned over it.

Tapping mode is another basic mode of operation that is widely used in atomic force microscopy. During operation, the cantilever vibrates at an appropriate frequency and is positioned above the surface of the sample. This tapping of the cantilever generates

a very small force that interacts with the sample, resulting in very low wear on the sample. However, the interaction between the tip and sample during tapping mode is still in the range of repulsion, similar to constant force mode.

Non-contact mode is a method used to measure atomic forces that does not come into contact with the surface of the sample. Instead, the tip is positioned at a distance from the surface, and the force between the tip and the sample is measured as the tip is scanned over the sample. Non-contact mode is the least destructive of all modes and is therefore preferred for very delicate samples. However, this mode is less sensitive than constant force mode and tapping mode (Geng et al., 2007).

For analyzing the surface characteristics of a sample, it can be done by drawing a line through the points of interest on the image obtained from an atomic force microscope. This provides information on the structure of the line, which indicates the depth, height, and roughness of the surface. We use the Root Mean Square (Rrms) value to describe the roughness of the surface area in question.

$$R_{rms} = \sqrt{\frac{1}{N}\sum_{i=1}^{N}(h_i - \hbar)^2} \tag{2.25}$$

2.4.4 UV-VIS Spectroscopy for Studying Optical Properties

UV-VIS Spectroscopy is a technique used to study the optical properties of materials and was first used for chemical analysis around 1930 (Yadav et al., 2011). It is considered to be the first type of absorption spectroscopy. The wavelength range used for UV falls between 190-400 nanometers and extends to the visible range which falls between 380-800 nanometers. The principle of light transmission is that when light travels and hits a material, some of it will be reflected back on the surface of the material and some will penetrate into the material. The light that penetrates will be partially absorbed and some of it will exit the material, as shown in Figure 2.27. The absorbed light can then be analyzed to determine the material's optical properties (Vijayan et al., 2008).

Figure 2.27

The Nature of Light Transmission through a Medium

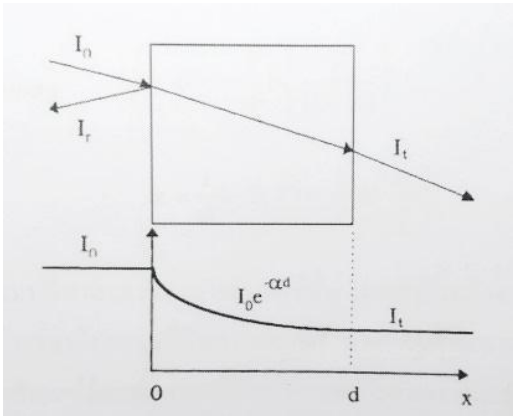

Source: (Boonnuk, 2011)

We can define the optical reflectivity coefficient (R), the optical absorption coefficient (α), and the optical transmittance coefficient (T) as follows:

$$R = \frac{I_r}{I_0} \tag{2.26}$$

Therefore, the intensity of light entering the object is

$$I_0 - I_r = I_0 - RI_0 = (1 - R)I_0 \tag{2.27}$$

Then, as light enters the material, it is absorbed. From the picture, you can see that light is valuable. The light intensity decreases exponentially with distance d.

In the case of reflection on the back surface, the intensity of the light that passes through the back of the material is

$$I_t = (1 - R)^2 I_0 e^{-\alpha d} \tag{2.28}$$

Light Penetration Coefficient

$$T = \frac{I_t}{I_0} = (1 - R)^2 e^{-\alpha d} \tag{2.29}$$

Absorption coefficient

$$\alpha = -\frac{1}{d}\ln\left[\frac{T}{(1-R)}\right] = \frac{1}{d} - \ln T = \frac{1}{d}\ln\left(\frac{I_0}{I}\right) \quad (2.30)$$

where I_0 is the light intensity incident on the material surface (W/m^2)
I_r is the light intensity reflected from the surface of the material (W/m^2).
I_t is the intensity of light that penetrates the surface of the material (W/m^2).

In studying the optical properties of organic materials, the energy levels in each range affect the changes within the molecules' different excited states. Measurements are affected in the range of gamma rays and X-rays, which result in electron transitions and the breakdown of bonds, leading to the details of the material structure analysis.

The range of far infrared radiation related to microwaves affects the rotation or movement of the molecules. The energy level in the range of ultraviolet radiation causes the electrons that create bonds to be in an excited state, resulting in delocalization of electrons and a decrease in the energy gap between HOMO and LUMO. This means that the energy used to excite electrons decreases, and the absorption of energy for this type of molecule occurs at lower frequencies.

When absorbing UV light, the appropriate amount of light causes electronic excitation from the ground state to the excited state. This means that electrons from energy levels with low energy will be stimulated to move to energy levels with higher energy, which is the energy absorbed. The energy difference (ΔE) between the excited state and the ground state of a molecule or atom is equal to the energy absorbed.

In excitation, the electrons of the sigma bond (σ-band) consume higher energy. This is because the energy range between the nonbonding orbitals and the bonding orbitals of the sigma bond is greater than that of the pi bond (π-band).

Molecules that absorb UV light with a wavelength of about 150 nanometers usually consist of cytosine because it is the energy that can excite electrons in cytosine. However, since the wavelength used is usually around 200-400 nanometers for UV and 200-800 nanometers for UV-visible spectroscopy, most molecules related to UV spectrophotometry contain pyrimidine.

Table 2.3

Values of Wavelength, Energy, and Type of Excitation

Spectral Region	Wavelength (nm)	Energy Range (cm^{-1})	Energy Range (eV)	Type of Excitation
Vacuum - UV	10 - 180	$1x10^6$ – 55,600	124 – 6.89	Electronic
UV	200 - 400	55,600 – 25,500	6.89 – 3.10	Electronic
Visible	400 - 750	25,500 – 13,300	3.10 – 1.65	Electronic
Near IR	750 – 2,500	13,300 – 4,000	1.65 – 0.50	Electronic, Vibrational, Overtones
IR	2,500 – 25,000	4,000 – 40,000	0.50 – 0.05	Vibrations, Phonons

2.5 Principles of Moisture Sensor Measurement

2.5.1 Humidity

Humidity refers to the amount of water present in the state of gas in the air or in other types of gas. The commonly used forms of humidity measurement are relative humidity, absolute humidity, and dew point temperature (Jalkanen et al., 2015). The relative humidity is the most widely used unit of measurement. The meaning of relative humidity is the ratio of the vapor pressure at that time to the saturated vapor pressure at the same temperature (Wang & Ye, 2008), usually expressed as a percentage in Equation (2.31).

$$\%RH = \frac{P_w}{P_s} \times 100 \tag{2.31}$$

where $\%RH$ is the relative humidity (%).

P_w is the partial pressure of steam (mbar).

P_s is the saturated steam pressure (mbar).

Absolute humidity is the ratio of the mass of water vapor to the volume of air or gas. It can be thought of as the density or concentration of water vapor in the air. It is expressed mathematically as shown in equation (2.32).

$$d_w = \left[\frac{M_w}{V_w + V_g} \right] = \frac{M_w}{V} \tag{2.32}$$

where d_w is the absolute humidity (kg/m^3).

M_w is the mass of steam (kg)

V_w is the volume of steam (m^3)

V_g is the volume of dry air (m^3)

V is the combined volume of steam and dry air (m^3)

The dew point temperature is the temperature at which the actual vapor pressure of the air or gas is equal to the saturated vapor pressure at that temperature, and the relative humidity is 100% (Matsuguchi et al., 2004). At this point, condensation begins to occur and the air or gas cannot hold any more water vapor. As the temperature drops below this point, the actual vapor pressure decreases continuously, while the saturated vapor pressure remains the same. This causes the actual vapor pressure in the air to be greater than the saturated vapor pressure, resulting in more condensation and the formation of droplets, similar to the phenomenon of water droplets forming around a glass containing ice. The temperature of the water in the glass is lower than the dew point temperature of the air at that time, causing condensation to occur on the surface of the glass. The dew point temperature changes with the pressure at that time.

In addition, humidity is also a measure of the amount of water in a gas or air in a gaseous state. It can be measured in terms of absolute humidity or relative humidity. Absolute humidity is a measure of the mass of water vapor compared to the total volume of dry air in the same space. However, relative humidity is the measure of the amount of water vapor in the air, expressed as a percentage of the maximum amount of water vapor that can be held in the air at the same temperature and pressure.

2.5.2 Humidity Sensor

The humidity sensor is a device that measures the amount of water vapor in the air and can indicate the amount of humidity in the air in the form of relative humidity. A good humidity sensor for various applications must have high sensitivity in a wide temperature and humidity range to provide accurate humidity values, low hysteresis, durability, compensate for temperature effects, respond quickly to changes in humidity, resist contamination, have a long service life, easy to connect to electronic circuits, have a simple structure, and be inexpensive (Korotcenkov, 2019). Various types of humidity sensors have been developed to suit different types of applications, which have different operating principles (Lee & Lee, 2005). For example, using moisture-absorbing materials, using a psychrometer, measuring dew point, or using infrared measurement. The selection of a sensor can be based on its size, weight, price, efficiency, or maintenance, and each method of humidity measurement has its advantages and disadvantages, as shown in Table 2.4.

Table 2.4

Comparison of Advantages and Disadvantages of Different Moisture Measurement Principles

Method	**Working Principle**	**Advantages**	**Disadvantages**
Moisture sensitive material	Utilizes changes in length, volume, or density	- No energy required -Non-directional response - Easy to use - Slow response time	- Slow response time - Requires periodic recalibration
	Utilizes materials that absorb or release moisture	-	-
The bulb method wet-dry	Take a temperature measurement wet-dry bulb	- No calibration required	- Need to change the filter and always adding distilled water - Requires air flow with a high flow rate
The dew point method	Measure the dew point temperature by detecting condensation using coolness	- High accuracy - Wide dynamic area - No calibration required	- Is large and expensive - High power consumption - Must be cleaned regularly
Measure by infrared radiation	Selective absorption infrared spectrum of steam	- Used with corrosive gases and wide dynamic area	- Expensive - Interference from other gas

2.6 Checking the Characteristics of a Moisture Sensor

2.6.1 Accuracy

Generally defined as the maximum error expected to occur between the reading and theoretical value. Sometimes this value is expressed as a percentage of the full-scale output (FSO) value. For example, a thermometer may guarantee accuracy within 5% FSO.

2.6.2 Sensitivity

Defined in terms of the relationship between input and output signals. Sensitivity is generally the ratio of the change in output to the change in input (Nowak et al., 2020). When the input changes slightly, sensitivity may be expressed as the derivative of the transfer function with respect to the input signal. The rate of change of the moisture sensor in relation to the moisture that changes is proportional to the humidity (McGhee et al., 2020) as shown in Equation (2.33).

$$S = \Delta Z / \Delta RH \tag{2.33}$$

Where S is the sensitivity of the humidity sensor (Ω / %RH)

ΔZ is the difference in the impedance during the measurement (Ω)

ΔRH is the difference in humidity during the measurement (%RH)

2.6.3 Linearity

The linearity of a sensor is seen from a graph showing the relationship between output and input that is close to a straight line, which may be a straight line in a narrow input range. Normally, the sensor is used only in the linear range.

2.6.4 Range

The range of a sensor determines the limitation in which the sensor can work effectively. Usually, the range is set by the minimum and maximum input values that can be measured. The range can vary with speed, meaning that if the range is narrow, the speed will be high, and if the range is wide, the speed will be low. It is essential not to measure outside the specified range because it can cause the device to fail or be damaged, or it may pose a risk to health or safety (Lee et al., 2006).

2.6.5 Resolution

The resolution of a sensor is related to the smallest input or the smallest change in input that it can detect. Normally, it is expressed in terms of the smallest increase in input that can be measured or detected. The higher the resolution of the display, the smaller the size of the measurement or detection (Duan et al., 2021). For example, a display that shows decimal numbers with 4 decimal places, 0.0001 units, has a higher resolution than a display that shows measurements with 3 decimal places, 0.001 units.

2.6.6 Response

The response rate to changes in humidity is tested by inputting humidity values in a step ladder pattern. Generally, the relative humidity is increased from 11% to 93% to test the response rate (Tetelin et al., 2003).

2.6.7 Frequency Response

The input given to the sensor may have a constant value or may change over time. The number of oscillations of a change in value in a given time unit is called frequency. Each type of sensor has different abilities to respond to frequency depending on the natural frequency of the sensor. Sensors with high natural frequencies can be used for both static and dynamic loads. Generally, sensors should have a natural frequency at least two times higher than the input signal frequency. The sensor should not be used to measure input signals that have frequencies close to or equal to the sensor's natural frequency because it may cause resonance and produce inaccurate results, potentially damaging the sensor.

2.6.8 Hysteresis

This is the maximum difference between the value read from the measuring device during the rising edge and the falling edge of the same point.

2.6.9 Repeatability

Repeatability is the ability to obtain the same value from multiple measurements under limited conditions. It is a measure of a sensor's ability to produce the same output or response for repeated measurements of the same quantity under the same conditions. Repeatability may provide the maximum positive and negative percentage deviation of readings or under each reading condition.

2.6.10 Stability

Stability measures the changes in output from a sensor under constant input over a long period of time.

2.6.11 Reliability

Reliability refers to the consistency of a sensor's output under different conditions, such as temperature, humidity, vibration, and so on. A reliable sensor produces the same output under similar conditions repeatedly (Sama et al., 2017).

2.6.12 Operating Life

The benefit of the operating life of a sensor is that it serves as an indicator of the period of time that the sensing element is expected to function under the specified conditions. The operating life is usually presented in terms of time, number of operations, or number of cycles that the sensor should withstand.

2.6.13 Dual Sensitivity

Typically, a sensor is designed to measure only one quantity, such as pressure, light, or force. However, some sensors may have dual sensitivity to other quantities, such as temperature or acceleration (Liu et al., 2017). If a sensing element is used to measure a quantity that changes with temperature, such as pressure, errors can arise due to dual sensitivity. This means that the sensor is measuring two quantities simultaneously.

CHAPTER 3
METHODOLOGY

This chapter discusses the preparation of thin films of titanium dioxide, changes in the conditions of titanium dioxide thin film formation, and the study of the effects of these conditions on various properties of the thin films. These properties include the structure of the films and the characteristics of their surfaces. After studying the properties of titanium dioxide, the article explains the principles of gas-phase deposition using an electron-beam evaporator in a vacuum system which is described in Figure 3.1.

Figure 3.1

Diagram Showing the Research Process

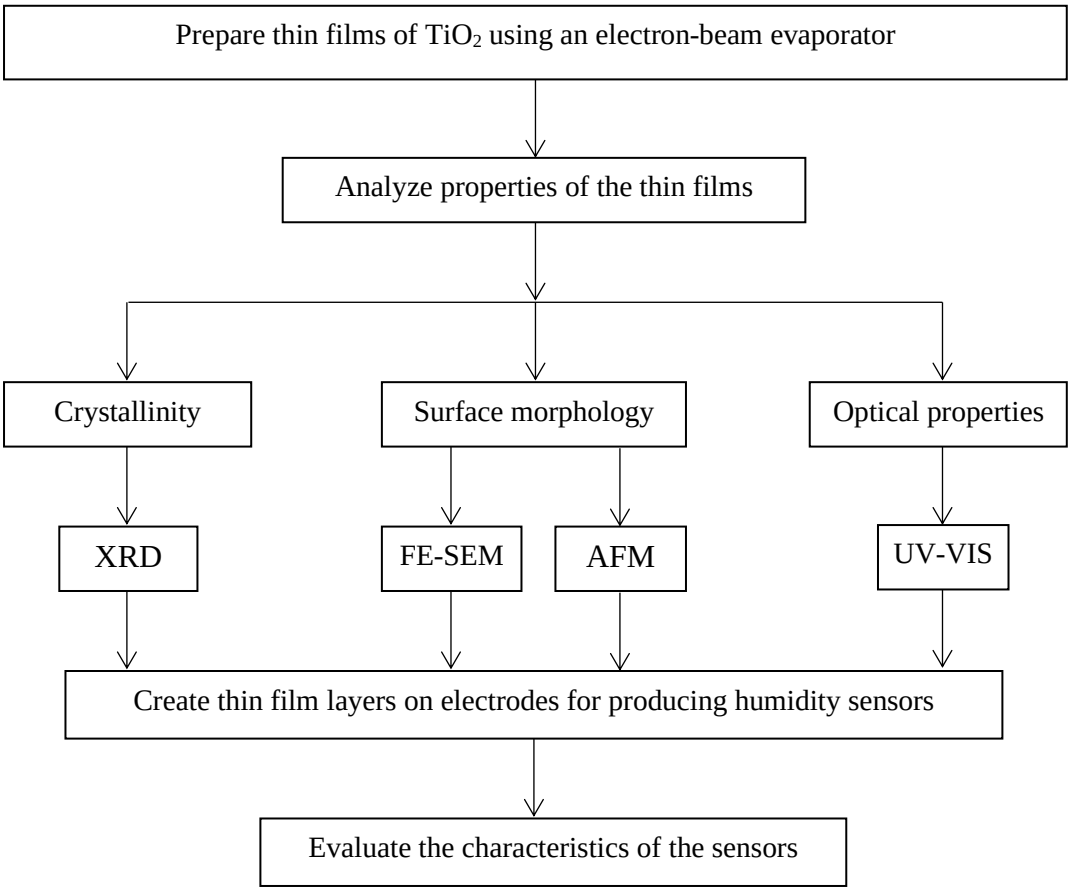

3.1 Preparation of Thin Films Using Electron-Beam Evaporation in a Vacuum System

Consider Figure 3.2, which shows a thin film preparation system under a pressure of 10^{-6} millibars using a rotary pump in combination with a turbo molecular pump. This thin film preparation system consists of a crucible made of graphite and four materials for evaporation: organic substances, inorganic substances, and metal electrodes. The shutter is used to control the release of the vapor from the crucible. The electron-beam evaporation system in a vacuum used in this research is shown in Figure 3.3.

Figure 3.2

System for Preparing Thin Films by Evaporation with Electron-Beam in Vacuum

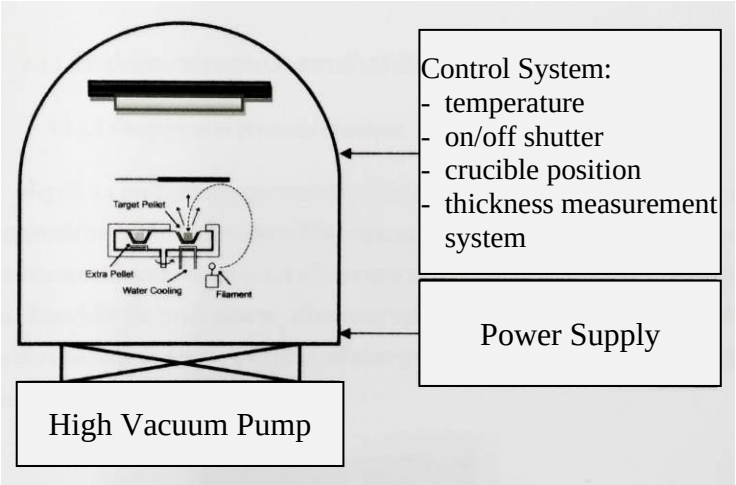

Figure 3.3

Electron-Beam Vacuum Deposition System

3.1.1 Components of the High Vacuum Electron-Beam Deposition System

3.1.1.1 **Vacuum Chamber.** As shown in Figure 3.4, the vacuum chamber contains the evaporation source, which is a device that heats the material to be evaporated in the crucible, causing it to change from a solid to a liquid or gas phase that coats the substrate. The system also includes a shutter for opening and closing the evaporation of material, a crystal monitor for measuring the thickness of the film, a substrate workholder for holding the substrate, a quartz lamp for heating the substrate, and a thermocouple.

Figure 3.4

The Inside of the Vacuum Container of the Film Preparation System

3.1.1.2 **Vacuum System and Pressure Measurement Equipment.** A mechanical rotary pump is used to create initial vacuum, which can create a vacuum from atmospheric pressure to about 10^{-3} millibars. The simple principle is that gas or air in the container is driven out by the movement of the piston, causing the gas in the suction chamber to increase in pressure until it is greater than the atmospheric pressure. The gas is then driven out.

A turbo molecular pump is used to create a vacuum from 10^{-3} to 10^{-10} millibars. The gas or air in the container is driven out by the rotation of the blades. The turbo molecular pump is composed of multiple layers of rotors and stators. The gas inside the container is driven out from the upper layer to the lower layer and then expelled outside.

3.1.1.3 **Gas System Control (Controller).** The gas system control, which is composed of an electron beam, includes:

1. A status control system for displaying pressure values within the chamber.
2. A thickness monitoring system that checks the thickness and deposition rate of the film while it is being evaporated in the chamber.
3. A turret control system that controls the rotation and positioning of the crucible.
4. A substrate control system that controls the temperature of the substrate holder.
5. A rotary workholder control system that controls the rotation of the workpiece holder.
6. A shutter control system that controls the opening and closing of the shutter.
7. A source control system that controls the electron beam source operation.
8. A sweep control system that controls the electron beam deflection.
9. The gas system control panel for the electron beam evaporation in a vacuum chamber is shown in Figure 3.5.

Figure 3.5

Control Panel of the Electron-Beam Evaporation System in the Atmosphere

3.1.1.4 **Power Supply.** This is the power source for the electron-beam generator of the electron-beam evaporation system in the atmosphere, which is appropriate for the organic substance evaporation.

3.1.1.5 **Adjustable Substrate Holder.** The substrate holder used in the Glancing Angle Deposition technique with angles of 0, 60, 70, and 80 degrees, as shown in Figure 3.6.

Figure 3.6

Substrate Holder Used for Electron Beam Evaporation with Glancing Angle Deposition Technique

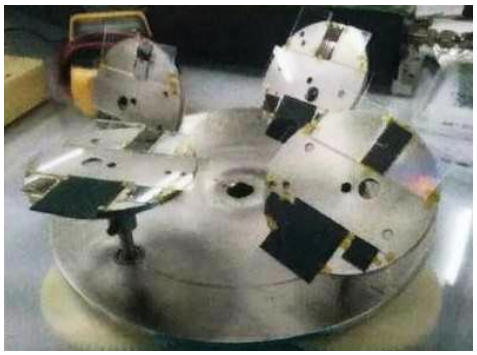

3.2 Substrate Preparation

To grow thin films, the first step is substrate preparation. In this experiment, a Silicon wafer was chosen as the substrate and cleaned to remove any oil and particle residues from transportation and long-term storage in a clean room (Class 100).

3.3 Titanium Dioxide Thin Film Growth

3.3.1 Steps and Conditions for Growing Thin TiO_2 Films

Thin films were grown using electron beam evaporation. The conditions for growing thin TiO_2 films were studied as follows:

3.3.1.1 **Substrate Angle Conditions at Various Angles.** Performing the deposition of material in a vacuum system under all conditions, with a pressure of approximately 2.6×10^{-6} mbar, using a P-type silicon substrate. A film is then deposited by heating the substrate to 100 degrees Celsius, with a thickness of 500 nanometers. The substrate is set at angles of 0, 60, 70, and 80 degrees. The resulting film is then subjected to structural characterization by measuring its X-ray diffraction pattern, examining its surface morphology and thickness using a scanning electron microscope, and testing its optical properties by measuring its light transmission. The film's

electrical properties are also tested by measuring its refractive index and conductivity under different conditions, as summarized in Table 3.1.

Table 3.1

Conditions for Depositing Titanium Dioxide Films on Substrates at Different Angles

Parameters for film preparation	Conditions for film preparation
Pressure	2.6×10^{-6} mbar
Thickness of thin film	500 nm
Angle of substrate	0, 60, 70, and 80 degrees
Deposition rate	0.05 nm/s
Substrate temperature	100 degrees Celsius

3.3.1.2 **Conditions for Annealing of Thin TiN Films.** Thin TiN films grown on various substrates were annealed in an atmosphere at the room temperature for 30 minutes. The resulting films were then characterized for their structural properties by measuring their X-ray diffraction patterns, examining their surface morphology and thickness using a scanning electron microscope, determining their optical properties by measuring their transmission spectra, and measuring their electrical properties. The annealing conditions are summarized in Table 3.2.

Table 3.2

Conditions for Baking Thin Films of Titanium Dioxide

Film preparation parameter	Conditions
Temperature	25 °C
Baking time	30 minutes
Atmosphere Ambient air	Vacuum

3.4 Preparation of Thin Film Tin-Dioxide Structure for Electrical Property Characterization

In this experiment, thin film tin-dioxide structures were prepared for electrical property characterization. The preparation process started with the preparation of a silicon substrate, which was then used to grow a thin film tin-dioxide under various conditions. After that, device fabrication was performed to facilitate the measurement of I-V and C-V characteristics. The resulting device is shown in Figure 3.8.

Figure 3.7

The Structure of the Thin Film Tin-Dioxide

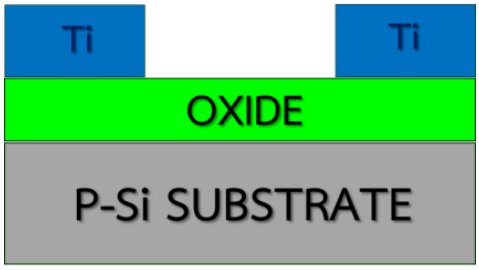

Figure 3.8

Apparatus for Measuring Electrical Properties

3.5 Characterization of Thin Film Tin-Dioxide Structure

3.5.1 X-Ray Diffraction Analysis for Structural Property Characterization

X-ray diffraction analysis was performed to investigate the structural properties of the thin film tin-dioxide structure. This method uses the principle of diffraction to analyze the structure of the sample. The resulting graph is a plot of the intensity of the X-ray diffraction against the angle of diffraction. Each element and compound has a unique diffraction pattern. In this experiment, an X-ray diffractometer from the Center of Microelectronics Technology (TMEC) was used for the analysis.

Figure 3.9

An X-Ray Diffractometer (XRD)

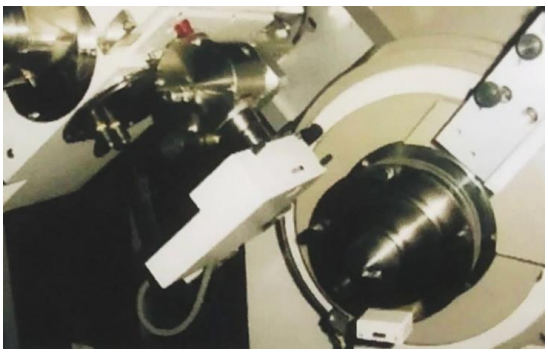

3.5.2 Discusses Examining Surface Characteristics Using a Field Emission Scanning Electron Microscope (FE-SEM)

The FE-SEM microscope is used to examine the surface characteristics of a sample. Electrons are scanned over the surface of the sample, and the resulting image is displayed on a CRT monitor. The image is black and white, with a magnification of 10-300,000 times, depending on the type of sample. The principle of operation is that the interaction of electrons with the sample produces secondary electrons, which are detected and amplified to create an image displayed on the monitor. The FE-SEM microscope is a device used by the Microelectronics Technology Center (TMEC) for measurement and inspection.

Figure 3.10

A Field Emission Scanning Electron Microscope (FE-SEM)

3.5.3 Surface Analysis Using Atomic Force Microscope (AFM)

The main component of the Atomic Force Microscope (AFM) system is the use of a cantilever to measure force. The cantilever is a stiff material with a sharp pointed tip that is attached at the end. It is usually made of a high-strength material such as Silicon nitride (Si_3N_4), with a length of 100-500 and a thickness of 0.5-5.0.

As shown in Figure 3.11, the tip at the end of the cantilever measures the force between the sample and the tip. The tip comes into contact with the sample surface with a force in the nanonewton range and moves along the surface of the sample, which is placed on a piezoelectric scanner. The scanner can control movement in three directions (x, y, and z axes). The tip moves up and down according to the height and depth of the sample surface, and the AFM system can measure the position of the tip by using a laser beam that is reflected back to a photodiode detector. This provides information about the up and down movement of the cantilever, and therefore the height and depth of the sample surface. By comparing the height information of each point with the position of the tip (x, y, and z coordinates), the AFM system can create a two-dimensional or three-dimensional image of the sample surface.

Figure 3.11

Principles of Operation of an Atomic Force Microscope (AFM)

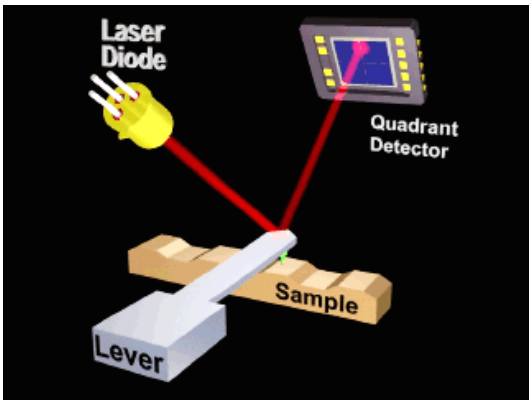

After examining the surface of a thin film, the roughness values under different conditions of the thin film will be analyzed. This will be done using an Atomic Force Microscope (AFM) from the Microelectronics Technology Research Center (TMEC), as shown in Figure 3.12.

Figure 3.12

Atomic Force Microscope (AFM)

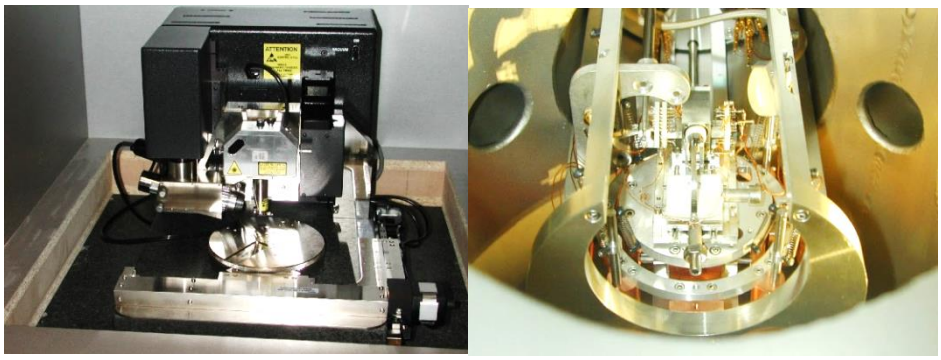

3.5.4 Checking Optical Properties with UV-VIS Spectroscopy

UV-VIS Spectrophotometer is a technique used for analyzing substances by measuring the absorption of light in the ultraviolet and visible ranges, approximately 190-1000 nanometers, of various chemical substances such as organic compounds, complex compounds, or inorganic compounds. The sample is placed in a sample holder and

positioned close to the light source. The sample absorbs or partially absorbs the light while the unabsorbed light passes through to the photomultiplier tube (PMT) detector. The amount of light that is absorbed is measured by subtracting the amount of light before absorption. The data is then processed into a spectrum that shows the relationship between the absorbance and the wavelength of light. The UV-VIS Spectrophotometer used in research is from the Nanotechnology College, King Mongkut's Institute of Technology Ladkrabang, and the Institute of Technology Ladkrabang.

Figure 3.13

A UV-VIS Spectrophotometer

3.6 Testing of Electrical Properties

This is a test to find the electrical properties of thin titanium dioxide films by measuring the basic electrical properties using the Agilent E4980A Precision LCR Meter, 20 Hz to 2 MHz. Various tests on thin titanium dioxide films will be studied from their electrical current, voltage and capacitance properties in order to determine the dielectric constant of thin nanotitanium dioxide films. Figure 3.14 shows the Agilent E4980A Precision LCR Meter, 20 Hz to 2 MHz at the Sirindhorn International Institute of Technology, King Mongkut's University of Technology Ladkrabang.

Figure 3.14

The Agilent E4980A Precision LCR Meter, 20 Hz to 2 MHz

To test the response of the sensors to varied humidity, the standard solutions, including LiCl, CH_3COOK, $MgCl_2$, $Mg(NO_3)_2$, NaCl, KCl, and KNO_3, contained in the bottles with the relative humidity of 11%, 23%, 33%, 52%, 75%, 85%, and 93%, respectively, were used and the capacitance values were measured by using LCR (Agilent E4980A Precision LCR Meter, 20 Hz to 2 MHz). In addition, the sensitivity of the TiO_2 films of varied frequencies have been calculated from the slope of the plots between the capacitance and the relative humidity (%RH).

CHAPTER 4

EXPERIMENTAL RESULTS

4.1 Results of the Characterization of Nanostructured Thin Films of Titanium Dioxide

The research results of the preparation and analysis of the properties of nanostructured thin films of titanium dioxide are presented. Thin films were prepared using the Glancing Angle Deposition (GLAD) technique at angles of 0, 60, 70, and 80 degrees with respect to different substrate angles. The thickness of the thin films was 500 nanometers, and the deposition was carried out at a source power of 10 kW. The thin films were annealed in air at the room temperature for 30 minutes.

The application of the nanostructured titanium dioxide thin films as humidity sensors was also investigated. The following details were studied:

1. Surface properties and thickness of the nanostructured titanium dioxide thin films used as humidity sensors.
2. Characteristics of the humidity sensors.

4.1.1 The Effect of the Angle between the Thin Film and the Substrate

The adjustment of the angle of a thin titanium dioxide film with the substrate was carried out to find the angle at which the thin film is under the most complete vacuum system, with the most uniform and homogeneous surface. The experiment used an electrical potential of 10 kilovolts, and the results are as follows.

The experiment analyzed the properties of a nano-sized titanium dioxide thin film by adjusting the angle of the thin film with the substrate at 0, 60, 70, and 80 degrees, respectively, according to the principle of X-ray diffraction. The analysis results are shown in Figure 4.1.

Figure 4.1

X-Ray Diffraction Patterns of Thin Films of Nanocrystalline Titanium Dioxide at Different Angles

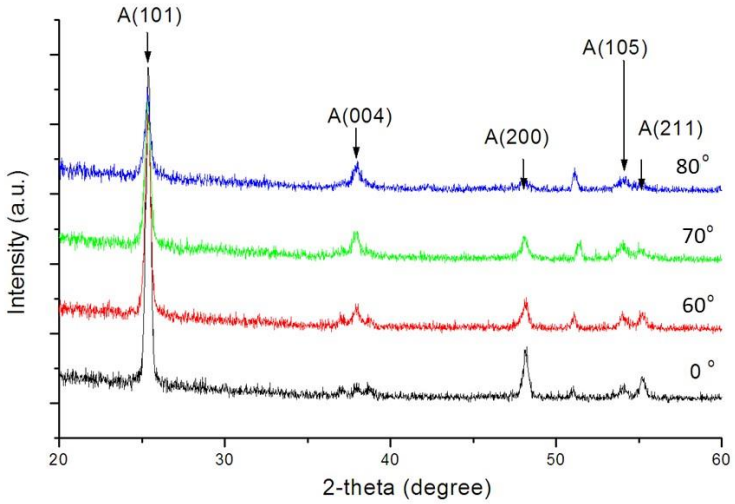

From Figure 4.1, the X-ray diffraction pattern exhibits bending peaks at angles of 25.4, 37.6, 47.5, 54.1, and 55.0 degrees, corresponding to the (101), (004), (200), (105), and (211) crystal planes, respectively. Analysis revealed that these are the bending planes of nanocrystalline titanium dioxide with an Anatase structure. The graph shows that as the angle between the thin film and the substrate increases, the thin film becomes more crystalline. The angle between the thin film and the substrate of 70 degrees indicates the highest crystallinity. This is because when the emitted electrons hit the substrate, the thick angles cause the material to pile up on the substrate. The aggregated crystallites will create a stronger peak when measured for the diffraction pattern. As the angle between the thin film and substrate decreases, the crystallinity of the film decreases in order.

In the experiment, the surface properties of thin films of titanium dioxide nanoparticles were analyzed by adjusting the angle between the thin film and the supporting base at 0, 60, 70, and 80 degrees, respectively. The surface morphology and structure were studied using a scanning electron microscope and an atomic force microscope. The results of the analysis are shown in Figure 4.2.

Figure 4.2

Photographs of the Surface and Cross-Section of Thin Films at Different Angles

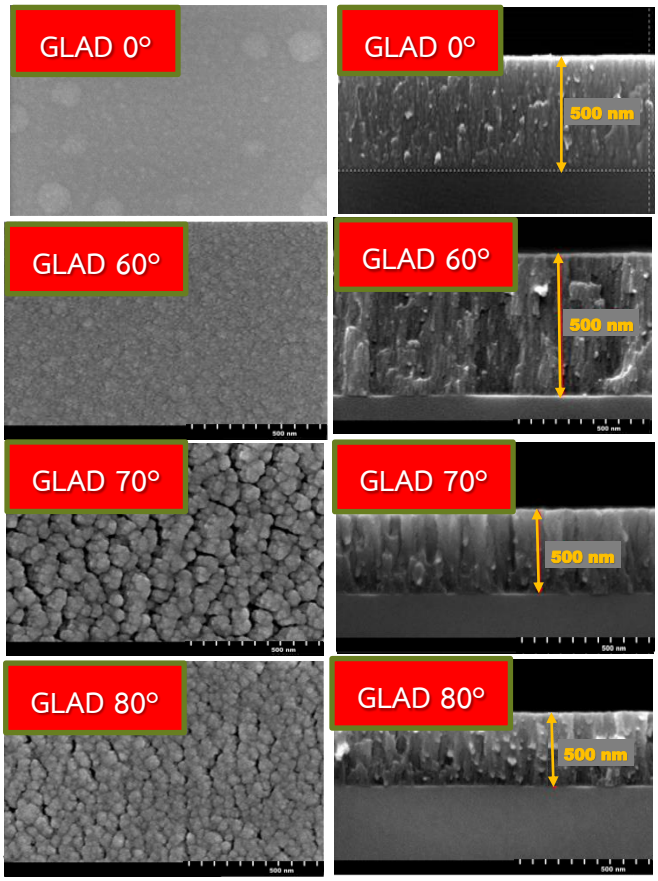

From Figure 4.2, it is found that the photographs taken from the scanning electron microscope and the transmission electron microscope show a grainy appearance on the film. The angle between the thin film and the support base is equal to 70 degrees, the angle between the thin film and the coated film on the support base, which allows for the best overlapping of the film on the support base. The distribution of the substance is well distributed, resulting in a uniform film and the highest level of graininess due to the large amount of overlapping of the substance. The film substance clumps together to form groups. Meanwhile, when the angle between the thin film and the support base is reduced, the film coated on the support base is better overlapped, and the substance distribution at an angle of 80 and 60 degrees between the thin film and the support base can be well distributed on the film. At a 0 degree angle between the thin film and the support base, it is found that some thin films are randomly distributed due to the lack of adjustment of the angle between the thin film and the support base, resulting in a

decrease in the amount of electron leakage at the base, and causing the substance to be irregularly distributed. In addition, in the cross-sectional photograph of some thin films, the thickness of the thin film layer is found to be equal to 500 nanometers.

4.1.2 The Effect of Room Temperature of Thin Films on Substrates

The results of room temperature of thin films of titanium dioxide on a substrate were obtained to find the temperature at which the thinnest film was produced under a highly vacuumed system with the best moisture absorption capability. The experiment was conducted using an electrical potential of 10 kilovolts and an angle between the thin film and the substrate of 70 degrees. The following are the results of the experiment:

In the experiment, the properties of the nanocrystalline titanium dioxide film were analyzed by adjusting the temperature for annealing the thin film on the substrate at room temperature to study the structural properties of the film using the principle of X-ray diffraction. The results of the analysis are shown in Figure 4.3.

Figure 4.3

The X-Ray Diffraction Patterns of the Nanocrystalline Titanium Dioxide Film at the Room Temperature of 70 Degrees

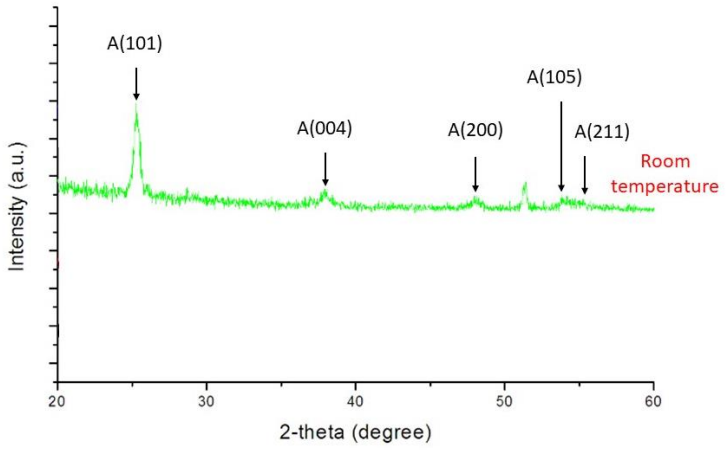

From Figure 4.3, it was found that the X-ray diffraction pattern showed bending angles at 25.4, 37.6, 47.5, 54.1, and 55.0 degrees, respectively, corresponding to the (101), (004), (200), (105), and (211) bending planes. Analysis revealed that this is the bending

plane of the nano-sized particle of titanium dioxide with the Anatase structure. The room temperature was found to give the highest crystallinity.

In the experiment, the surface properties of the prepared nano-sized titanium dioxide thin film were analyzed by adjusting the temperature of the thin film during annealing on the substrate to room temperature. This was done to investigate the surface properties and crystal structure using a transmission electron microscope and an atomic force microscope. The results of the analysis are shown in Figure 4.4.

Figure 4.4

Photographs of the Surface of Thin Films at the Room Temperature of 70 Degrees

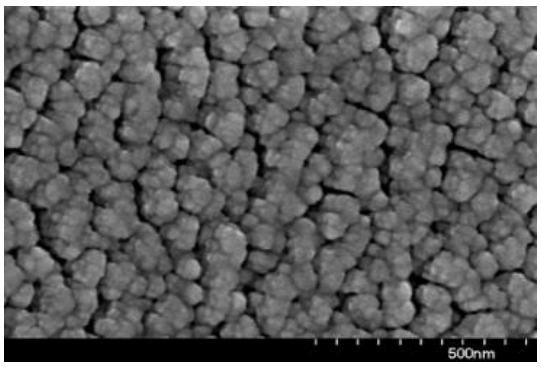

From Figure 4.4, it can be observed that thin films have different characteristics of cracks and pores. The temperature at which some thin films are baked on the substrate is the room temperature. Thin films coated on the substrate can be overlapped and dispersed the material well, resulting in a uniform texture and the highest degree of cracks and pores. This is because there is a large amount of material overlap, causing the film texture to clump together. In this type of crack and pore, the film should have better moisture absorption characteristics on the supporting base.

4.2 Examining the Specific Characteristics of the Humidity Sensor

4.2.1 Results of Optical Properties Examination

In the experiment of testing the optical properties of the thin TiO_2 films, the distances between the tips and bases were varied as 20, 30, and 40 mm to study the light properties using UV-VIS spectroscopy. The result of the optical properties is show in Figure 4.5.

Figure 4.5

The Light Absorbance of the Thin TiO_2 Films

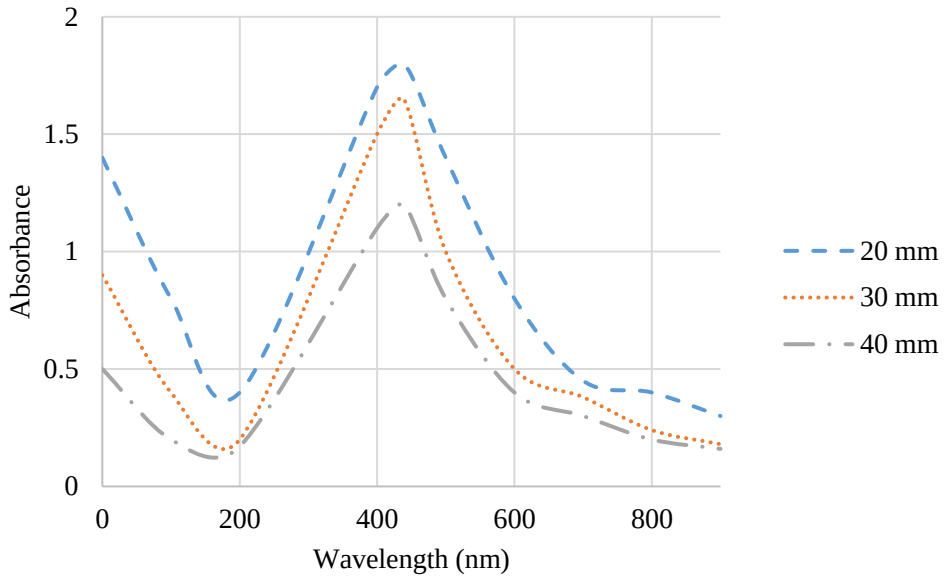

According to Figure 4.5, the experiment measured the absorbance of the light in the wavelengths of 300 to 900 nm. It was found that the peak of the absorbance is at 436 nm, following to the surface plasmon resonance (SPR). Moreover, the absorbance increases when the distances between the tips and bases are decreased due to the increased thickness of the thin films.

4.2.2 Results of Electrical Properties Examination

In the experiment, capacitance values will be measured at frequencies of 100 Hz, 500 Hz, 1 kHz, and 2 kHz, respectively. The relative humidity values of different nanotitanium dioxide thin films will be measured. The angle between the thin film and the substrate are 60, 70, 80 degrees, and the temperature during the annealing process of the thin film on the substrate is 25 degrees Celsius. The results of the experiment show electrical properties as illustrated in Figures 4.6, 4.7, and 4.8, respectively.

Figure 4.6

The Examination of the Characteristics of Sensors with Different Relative Humidity and Temperatures during Baking on a Thin Film with 60 Degrees on a Supporting Base at the Room Temperature, with Varying Frequencies

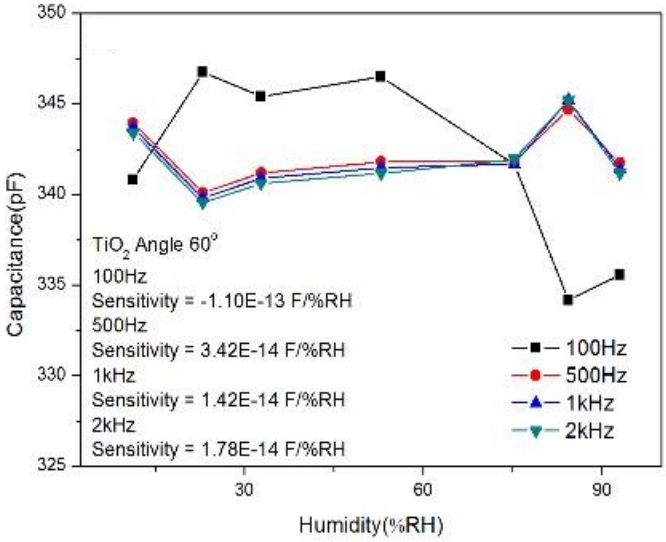

Figure 4.7

The Examination of the Characteristics of Sensors with Different Relative Humidity and Temperatures during Baking on a Thin Film with 70 Degrees on a Supporting Base at the Room Temperature, with Varying Frequencies

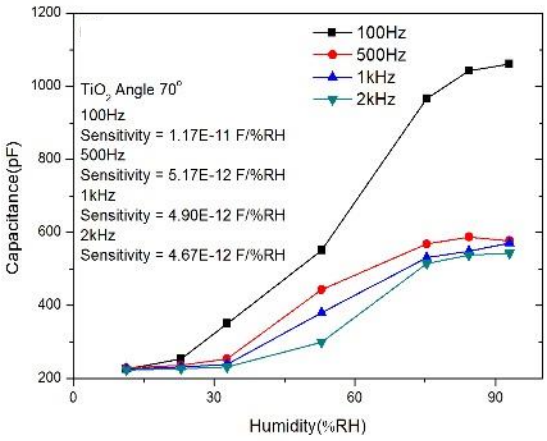

Figure 4.8

The Examination of the Characteristics of Sensors with Different Relative Humidity and Temperatures during Baking on a Thin Film with 80 Degrees on a Supporting Base at the Room Temperature, with Varying Frequencies

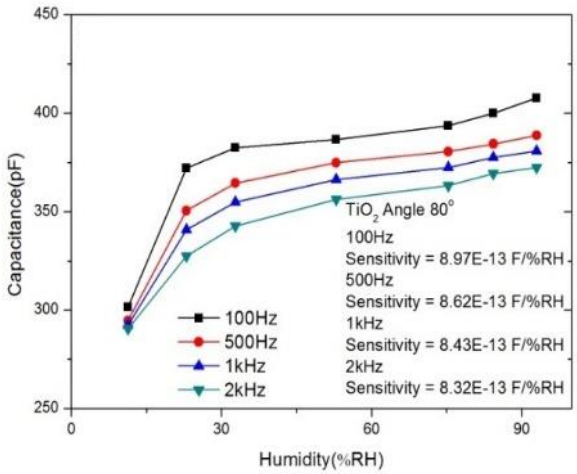

From Figures 4.6, 4.7, and 4.8, it is found that at lower frequencies, the capacitance value increases as the relative humidity increases. This low frequency causes better absorption of water molecule which leads to an increase in polarization. Higher relative humidity causes water ions to attach more to the sensor area, allowing for better conductivity. In addition, the response of the capacitance value of the sensor may come from the good surface properties of the thin film. The surface of the nanotitanium dioxide film can absorb water molecules well, and as relative humidity increases, the absorption of water molecules on the surface of the film increases. Water molecules also create dipole moments, leading to an increase in dielectric constant and charge storage values of the humidity sensor. In summary, as the relative humidity increases, the capacitance value increases due to the increase in the number of dipole moments in the absorption of water molecules.

When comparing the differences in measuring relative humidity of prepared nanotitanium dioxide thin films, at the angles of 60, 70, and 80 degrees between the thin film and the substrate, and at the room temperatures for the thin film on the substrate, it can be observed from the linear relationship shown in Figures 4.6, 4.7, and 4.8 that a good humidity sensor can be determined. Therefore, it can be seen that at the

angle of 70 degrees and at the room temperature for the thin film on the substrate, it exhibits the best linear characteristics for a good humidity sensor because it can distinguish humidity levels at all frequencies and percentages of relative humidity (%RH).

CHAPTER 5
CONCLUSIONS

The preparation of thin films of titanium dioxide nanoparticles was achieved by using electron beam evaporation with nanotechnology. The effect of applying a 10 kW electrical potential with different substrate angles was investigated. The Glancing Angle Deposition (GLAD) technique was used with a 70 degree angle, and the films were annealed at the room temperature for 30 minutes in the air to ensure complete annealing. The analysis of the dispersion conditions of the particles revealed that the thin films prepared from the titanium dioxide nanoparticles had an anatase crystal structure with planes (101), (004), (200), (105), and (211) present. The surface properties of the thin films were found to be homogeneous upon inspection. The light properties of the films were investigated, and it was found that the thin films of titanium dioxide nanoparticles exhibited a surface plasmon resonance phenomenon, causing the absorption of light.

The invention of a humidity sensor, it can be prepared from conditions in preparing thin films. The thickness of the thin film of nanoscale titanium dioxide particles is 500 nanometers. When analyzing the response value to measure humidity, it was found that the sensor responded to humidity in the range of 11%RH - 93%RH with a very good range of response. As the relative humidity increased, the impedance value decreased because the increased amount of water vapor caused it to adhere more to the sensor, resulting in the movement of the electrons of the sensor being able to move more efficiently. When analyzing the response time to absorption and desorption of humidity, it was found that the sensor had a very good response time of 3.5 and 2.0 seconds, respectively. Upon checking the stability of the sensor, it was found that after 30 days, the impedance values of the sensor for all humidity levels were significantly lower, indicating good stability of the sensor and accuracy in measuring and operating in the future.

From the analysis of the electrical properties testing, it was found that at low frequencies there is a clear variation in the capacitance values due to the effect of polarization. However, when the frequency is increased, there is not much change in

the capacitance values. Additionally, when tested in the form of an electrical capacitor, it was found that at low frequencies, the capacitance values are high, and as the relative humidity increases, the polarization effect increases. Furthermore, the response of the capacitance value of the sensor comes from the properties of the nanoparticles, where the surface of the nanotitanium dioxide film can absorb water molecules very well, which increases the polarization effect. As the humidity increases, the absorption of water molecules on the surface of the film becomes greater, resulting in a larger dipole moment and a higher dielectric constant and capacitance value in the moisture detection measurement. Finally, when analyzing the circuit characteristics using the complex impedance method, the equivalent circuit or model of the sensor can be determined for designing the device for future use.

In summary, the advantages of the humidity microsensors based on the thin TiO_2 films are that they can more precisely, accurately, and rapidly measure humidity in the air. The applications of the humidity microsensors with the thin TiO_2 films are for humidity measurements in places where the humidity needs to be rigidly controlled, such as the industry of pharmaceutical manufacturing, furniture manufacturing, and rice production. However, there are some limitations of this work. Firstly, the size of the created sensors is still large, and it could be smaller than the created sensors when using the future material technologies. Secondly, the thickness of the thin film of nanoscale titanium dioxide particles is limited as of 500 nm in this work. In the future, the thickness can be varied to experiment and use in various applications. Moreover, the scales of Glancing Angle Deposition (GLAD) angles were varied at only 0, 60, 70, and 80 degrees. Those scales can be more neatly varied in the future experiments to identify the most optimal GLAD angle. Lastly, the response humidity range of the constructed sensors are only between 11%RH - 93%RH, which may be too narrow in the real applications. Thus, other materials in the thin films and growing techniques can be used to enhance the response humidity range of the sensors.

REFERENCES

Akbari-Saatlu, M., Procek, M., Mattsson, C., Thungström, G., Nilsson, H., Xiong, W., Xu, B., Li, Y., & Radamson, H. H. (2020). Silicon nanowires for gas sensing: A review. *Nanomaterials*, 10, 2215.

Aneesh, R. & Khijwania, S. K. (2012). Titanium dioxide nanoparticle based optical fiber humidity sensor with linear response and enhanced sensitivity. *Applied Optics*. 51, 2164-2171.

Barrettino, D., Graf, M., Song, W.H., Kirstein, K.U., Hierlemann, A., & Baltes, H. (2004). Hotplate-base monolithic CMOS Microsystems for gas detection and material characterization for operating temperatures up to 500 °C. *IEEE Journal of Solid State Circuits*, 39(7), 1202-1207. https://doi.org/10.1109/JSSC.2004.829929

Boonnuk, Y. (2011). *Preparation of silver nanoparticle thin films by electrostatic spray deposition for humidity sensors* [Master's thesis, King Mongkut's University of Technology Ladkrabung].

Dai, C.L., Peng, H.J., Liu, M.C., Wu, C.C., Hsu, H.M., & Yang, L.J. (2005) A micromachined microware switch fabricated by the complementary metal-oxide semiconductor post-process of etching silicon dioxide. *Japanese Journal of Applied Physics*, 44, 6804-6809. https://doi.org/10.1143/JJAP.44.6804

Dai, C.L. & Yu, W.C. (2006). A micromachined tunable resonator fabricated by the CMOS post-process of etching silicon dioxide. *Microsystem Technology*, 12, 766-772. https://doi.org/10.1007/s00542-005-0077-8

Das, J., Dey, S., Hossain, S.M., Rittersma, Z.M.C., & Saha, H. (2003). A hygrometer comprising a porous silicon humidity sensor with phase-detection electronics. *IEEE Sensors Journal*, 3(4), 414-420. https://doi.org/ 10.1109/JSEN.2003.816261

Duan, Z., Jiang, Y., & Tai, H. (2021). Recent advances in humidity sensors for human body related humidity detection. *Journal of Materials Chemistry C*, 9, 14963 – 14980.

Fang, Z., Zhao, Z., Wu, Y., Zhang, B., & Wang, Y.Z. (2004). Integrated temperature and humidity sensor based MEMS, *Proceedings of the International*

Conference on Information Acquisition, 84-87. https://doi.org/10.1109/ICIA.2004.1373325

Furjes, P., Kovacs, A., Ducso, Cs., Adam, M., Muller, B., & Mescheder, U. (2003). Porous silicon-based humidity sensor with interdigital electrodes and internal heaters. *Sensors and Actuators B: Chemical*, 95, 140-144.

Geng, W., Wang, R., Li, X., Zou, Y., Zhang, T., Tu, J., He, Y., & Li, N. (2007). Humidity sensitive property of Li-doped mesoporous silica SBA-15, *Sensors and Actuators B: Chemical*. 127(2), 323-329. https://doi.org/10.1016/j.snb.2007.04.021

Jalkanen, T., Määttänen, A., Mäkilä, E., Tuura, J., Kaasalainen, M., Lehto, V., Ihalainen, P., Peltonen, J., & Salonen, J. (2015). Fabrication of porous silicon based humidity sensing elements on paper. *Journal of Sensors*, 2015, 1-10. https://doi.org/10.1155/2015/927396

Korotcenkov, G. (2019). *Handbook of humidity measurement, vol. 2: Electronic and electrical humidity sensors*. CRC Press.

Kraus, F., Cruz, S., & Muller, J. (2003). Plasma polymerized silicon organic thin films from HMDSN for capacitive humidity sensors. *Sensors and Actuators B: Chemical*, 88, 300-311. https://doi.org/10.1016/S0925-4005(02)00373-8

Ku, C. & Chung, C. (2023). Advances in humidity nanosensors and their application: Review. *Sensors*, 23, 2328.

Kuzubasoglu, B. A. (2022). Recent studies on the humidity sensor: A mini review. *ACS Applied Electronic Materials*, 4, 4797 – 4807.

Lee, C.Y. & Lee, G.B. (2005). Humidity sensors: a review. *Sensor Letters*, 3, 1-4. https://doi.org/10.1166/sl.2005.001

Lee, C.Y., Lin, C.H., Fu, L.M. (2006). Techniques in MEMS devices for micro humidity sensors and their applications. In: Leondes, C.T. (eds) MEMS/NEMS. Springer, Boston, MA. https://doi.org/10.1007/0-387-25786-1_27

Liu., M., Wang, C., & Kim, N. (2017). High-sensitivity and low-hysteresis porous MIM-type capacitive humidity sensor using functional polymer mixed with TiO_2 microparticle. *Sensors*, 17, 284.

Matsuguchi, M., Yoshida, M., Kuroiwa, T., & Ogura, T. (2004). Depression of a capacitive-type humidity sensor's drift by introducing a cross-linked structure in the sensing polymer. *Sensors and Actuators B: Chemical*, 102(1), 97-101. https://doi.org/10.1016/j.snb.2003.12.061

McGhee, J.R., Sagu, J. S., Southee, D. J., Evans, P. S. A., & Wijayantha, K. G. U. (2020). Printed, fully metal oxide, capacitive humidity sensors using conductive indium Tin oxide inks. *ACS Applied Electronic Materials*, 2 (11), 3593 – 3600.

Miao, Y., Lin, H., Li, B., Dong, T., He, C., Du, J., Zhao, X., Zhou, Z., Su, J., Wang, H., Dong, Y., Lu, B., Dong, L., & Radamson, H. H. (2023). Review of Ge(GeSn) and InGaAs avalanche diodes operating in the SWIR spectral region. *Nanomaterials*, 13, 606.

Miao, Y., Wang, G., Kong, Z., Xu, B., Zhao, X., Luo, X., Lin, H., Dong, Y., Lu, B., Dong, L., Zhou, J., Liu, J., & Radamson, H. H. (2021). Review of Si-based GeSn CVD growth and optoelectronic applications. *Nanomaterials*, 11, 2556.

Niarchos, G., Dubourg, G., Afroudakis, G., Georgopoulos, M., Tsouti, V., Makarona, E., Crnojevic-Bengin, V., & Tsamis, C. (2017). Humidity sensing properties of paper substrates and their passivation with ZnO nanoparticles for sensor applications. *Sensors*, 17(3), 516. https://doi.org/10.3390/s17030516

Nowak, P., Maziarz, W., Rydosz, A., Kowalski, K., Ziabka, M., & Zakrzewska, K. (2020). SnO_2/TiO_2 thin film n-n heterostructures of improved sensitivity to NO_2. *Sensors*, 20, 6830.

Samà, J., Seifner, M. S., Domènech-Gil, G., Santander, J., Calaza, C., Moreno, M., Gràcia, I., Barth, S., & Romano-Rodríguez, A. (2017). Low temperature humidity sensor based on Ge nanowires selectively grown on suspended microhotplates. *Sensors and Actuators B: Chemical*, 243, 669–677.

Shi, J., Hsiao, V. K.S., Walker, T. R., & Huang, T. J. (2008). Humidity sensing based on nanoporous polymeric photonic crystals. *Sensors and Actuators B: Chemical*, 129(1), 391-396. https://doi.org/10.1016/j.snb.2007.08.037

Tetelin, A., Pellet, C., Laville, C., & N'Kaoua, G. (2003). Fast response humidity sensors for a medical microsystem. *Sensors and Actuators B: Chemical*, 91(1-3), 211-218. https://doi.org/10.1016/S0925-4005(03)00090-X

Vijayan, A., Fuke, M., Hawaldar, R., Kulkarni, M., Amalnerkar, D., & Aiyer, R.C. (2008). Optical fibre based humidity sensor using Co-polyaniline clad, *Sensors and Actuators B: Chemical*. 129(1), 106-112. https://doi.org/10.1016/j.snb.2007.07.113

Vrakatseli, V. E., Kalarakis, A. N., Kalampounias, A. G., Amanatides, E. K., & Mataras, D. S. (2018). Glancing angle deposition effect on structure and light-induced wettability of RF-sputtered TiO_2 thin films. *Micromachines*, 9, 389.

Wang, X. & Ye, M. (2008). Hysteresis and nonlinearity compensation of relative humidity sensor using support vector machines, *Sensors and Actuators B: Chemical*, 129(1), 274-284. https://doi.org/10.1016/j.snb.2007.08.005

Xiaowei, L., Zhengang, Z., Tuo, L., & Xin, W. (2011). Novel capacitance-type humidity sensor based on multi-wall carbon nanotube/SiO_2 composite films. *Journal of Semicoductors*. 32(3), 034006.

Yadav, B. C., Singh, M., & Dwivedi, C. D. (2011). Optical characterization and humidity sensing properties of praseodymium oxide, *Sensors & Transducers Journal*. 125(2), 68-75.

VITA

Name: Lieutenant Colonel Phenthai Phinmuang

Education: 1. B.S. (Physics), Faculty of Science, Srinakharinwirot University, Thailand
2. M.S. (Physics), Faculty of Science, Chulalongkorn University, Thailand

Workplace: Department of Physics, Academic Division,
Chulachomklao Royal Military Academy, Thailand

E-mail: phenthai.ph@crma.ac.th